

Structural connectivity of thalamic subnuclei in major depressive disorder: an ultra-high resolution diffusion MRI study at 7-Tesla Liu, W.; Heij, J.; Liu, S.; Liebrand, L.; Caan, M.; van der Zwaag, W.; ...; van Wingen, G.

Citation

Liu, W., Heij, J., Liu, S., Liebrand, L., Caan, M., Van der Zwaag, W., ... Van Wingen, G. (2025). Structural connectivity of thalamic subnuclei in major depressive disorder: an ultrahigh resolution diffusion MRI study at 7-Tesla. *Journal Of Affective Disorders*, 370, 412-426. doi:10.1016/j.jad.2024.11.009

Version: Publisher's Version

License: <u>Creative Commons CC BY-NC 4.0 license</u>

Downloaded from: https://hdl.handle.net/1887/4258183

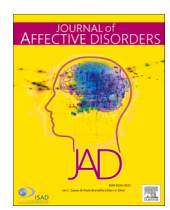
Note: To cite this publication please use the final published version (if applicable).

ELSEVIER

Contents lists available at ScienceDirect

Journal of Affective Disorders

journal homepage: www.elsevier.com/locate/jad



Research paper



Structural connectivity of thalamic subnuclei in major depressive disorder: An ultra-high resolution diffusion MRI study at 7-Tesla

Weijian Liu ^{a,b,c,*}, Jurjen Heij ^{d,e}, Shu Liu ^l, Luka Liebrand ^{b,f}, Matthan Caan ^{b,g}, Wietske van der Zwaag ^{d,e}, Dick J. Veltman ^h, Lin Lu ^{c,i,j,**}, Moji Aghajani ^{h,k,1}, Guido van Wingen ^{a,b,1,*}

- ^a Amsterdam UMC location University of Amsterdam, Department of Psychiatry, Amsterdam, the Netherlands
- ^b Amsterdam Neuroscience, Amsterdam, the Netherlands
- ^c Peking University Sixth Hospital, Peking University Institute of Mental Health, NHC Key Laboratory of Mental Health (Peking University), National Clinical Research Center for Mental Disorders (Peking University Sixth Hospital), Chinese Academy of Medical Sciences Research Unit (No. 2018RU006), Peking University, Beijing, China
- ^d Spinoza Centre for Neuroimaging, KNAW, Amsterdam, the Netherlands
- ^e Netherlands Institute for Neuroscience, KNAW, Amsterdam, the Netherlands
- ^f Amsterdam UMC location Vrije Universiteit Amsterdam, Department of Radiation Oncology, Amsterdam, the Netherlands
- g Amsterdam UMC location University of Amsterdam, Department of Biomedical Engineering & Physics, Amsterdam, the Netherlands
- ^h Amsterdam UMC location Vrije Universiteit Amsterdam, Department of Psychiatry, Amsterdam, the Netherlands
- i Peking-Tsinghua Centre for Life Sciences and PKU-IDG/McGovern Institute for Brain Research, Peking University, Beijing, China
- ^j National Institute on Drug Dependence and Beijing Key Laboratory of Drug Dependence, Peking University, Beijing, China
- k Institute of Education & Child Studies, Section Forensic Family & Youth Care, Leiden University, the Netherlands
- ¹ Key Laboratory of Genetic Evolution & Animal Models, National Research Facility for Phenotypic & Genetic Analysis of Model Animals (Primate Facility), National Resource Center for Non-Human Primates, Kunming Institute of Zoology, Chinese Academy of Sciences, Kunming, China

ARTICLE INFO

ABSTRACT

Keywords:
Ultra-high resolution diffusion MRI
7.0 Tesla
Thalamic subnuclei
Structural connectivity
Major depressive disorder

Background: The thalamus serves as a central relay station within the brain, and thalamic connectional anomalies are increasingly thought to be present in major depressive disorder (MDD). However, the use of conventional MRI scanners and acquisition techniques has prevented a thorough examination of the thalamus and its subnuclear connectional profile. We combined ultra-high field diffusion MRI acquired at 7.0 Tesla to map the white matter connectivity of thalamic subnuclei.

Methods: Fifty-three MDD patients and 12 healthy controls (HCs) were involved in the final analysis. FreeSurfer was used to segment the thalamic subnuclei, and MRtrix was used to perform the preprocessing and tractography. Fractional anisotropy, axial diffusivity, mean diffusivity, radial diffusivity, and streamline count of thalamic subnuclear tracts were measured as proxies of white matter microstructure. Bayesian multilevel model was used to assess group differences in white matter metrics for each thalamic subnuclear tract and the association between these white matter metrics and clinical features in MDD.

Results: Evidence was found for reduced whiter matter metrics of the tracts spanning from all thalamic subnuclei among MDD versus HC participants. Moreover, evidence was found that white matter in various thalamic subnuclear tracts is related to medication status, age of onset and recurrence in MDD.

Conclusions: Structural connectivity was generally reduced in thalamic subnuclei in MDD participants. Several clinical characteristics are related to perturbed subnuclear thalamic connectivity with cortical and subcortical circuits that govern sensory processing, emotional function, and goal-directed behavior.

^{*} Corresponding authors at: Amsterdam UMC, location AMC, Meibergdreef 5, 1100 DD Amsterdam, the Netherlands.

^{**} Corresponding author at: Institute of Mental Health/National Clinical Research Center for Mental Disorders/Peking University Sixth Hospital, Peking University, HuayuanBei Road 51, 100191 Beijing, China.

E-mail addresses: w.liu1@amsterdamumc.nl (W. Liu), linlu@bjmu.edu.cn (L. Lu), g.a.vanwingen@amsterdamumc.nl (G. van Wingen).

 $^{^{\}rm 1}$ Moji Aghajani & Guido van Wingen are shared senior authors.

1. Introduction

Major depressive disorder (MDD) is a prevalent condition that significantly impairs psychosocial functioning, diminishes the quality of life, and poses a substantial disease burden on society (Belmaker, 2008; World Health Organization, 2008). Despite significant advances in neurobiological research in MDD, a full understanding of its pathophysiology remains elusive (Malhi and Mann, 2018; Otte et al., 2016). Previous evidence supports that the thalamus is involved in the development of depression (Kempton et al., 2011; Nugent et al., 2013; Young et al., 2004; Zhang et al., 2022). The thalamus functions as a central hub within cortical networks, simultaneously modulating the activity of cortical regions and serving as a relay station for sensory information entering and exiting the cerebral cortex, thus playing a pivotal role in the transmission of sensory signals throughout the brain (Modha and Singh, 2010; Saalmann et al., 2012). Furthermore, through its rich connections with subcortical territories, the thalamus also plays a significant role in emotional processing (Barson et al., 2020; Pessoa, 2017). In comparison to healthy individuals, MDD patients demonstrate significant reductions in the volume of the overall left thalamus, as well as several left-sided thalamic nuclei (Chibaatar et al., 2023; Kempton et al., 2011; Nugent et al., 2013). In addition, patients with MDD exhibit altered functional connections characterized by heightened bottom-up thalamic inputs to various cortical and subcortical regions and diminished top-down connections from these regions to the thalamus, indicating an imbalance between excessive sensory information processing and insufficient suppression of negative emotions (Yang et al., 2022). Heightened network functional connectivity was observed in both the primary somatosensory cortex and the thalamus (Kang et al., 2018), with a positive correlation found between thalamic-temporal connectivity and the severity of symptoms in individuals with depression (Brown et al., 2017). The application of deep learning techniques has also revealed thalamic hyperconnectivity as a prominent neurophysiological characteristic of depression (Gallo et al., 2023).

Diffusion MRI (dMRI) studies have shown that patients with MDD exhibit significantly lower fractional anisotropy (FA) values in the right anterior thalamic radiation, as well as lower axial diffusivity (AD) values in bilateral anterior thalamic radiation, compared to health controls (HCs) (Lai and Wu, 2014). The FA values in the genu and splenium of the thalamic radiation are positively correlated with the severity of anxiety symptoms (Coloigner et al., 2019). Decreased mean diffusivity (MD) in thalamic radiation is associated with an increase in depressive symptom severity (Shen et al., 2019). Additionally, there is a negative correlation between the FA value of the right anterior thalamic radiation and illness duration (Lai and Wu, 2014). Dysfunctional frontal-limbic circuits, as evidenced by white matter reduction in the genu of the corpus callosum extending to the posterior thalamic radiation, have been confirmed to play a role in the pathophysiology of depression (Coloigner et al., 2019). At the large-scale network level, thalamus-related structural connectivity is abnormal in MDD patients (Zhang et al., 2022). As a central relay station that connects almost all regions of the brain through white matter fibers and is closely associated with emotion regulation, we focused on the thalamus to investigate the alterations of white matter microstructure in patients with MDD.

The thalamus is composed of many subnuclei, and different subnuclei have different fiber connections, which are tentatively implicated in different pathophysiological mechanisms of depression (Iglesias et al., 2018). Prior work on thalamic white matter connectivity, however, has almost exclusively employed standard field strength MRI (1.5/3.0 Tesla) and probed the thalamus as a whole, overlooking its subnuclear composition. Although greater intensity inhomogeneities may affect the reliability of the extracted metrics, the use of Ultra-High Field (UHF) MRI (7.0 Tesla) allows increased spatial resolution due to the higher signal-to-noise ratio (Cattarinussi et al., 2021; Liebrand et al., 2020; Vu et al., 2015), enabling improved subnuclei segmentation and more precise and reliable reconstruction of white matter parameter maps

(Strotmann et al., 2014; Zheng et al., 2021). Diffusion imaging tensor (DTI) data acquired at 7.0 Tesla greatly improves the subsequent fitting of data to the diffusion tensor model compared to 3.0 Tesla, thereby reducing the uncertainty in tensor estimation (Polders et al., 2011). The benefits of higher field strengths also translate to improved functional sensitivity, as UHF fMRI revealed disrupted emotion-related neural circuits in patients with MDD that could not be captured by 3.0 Tesla fMRI (Morris et al., 2019). Thus, 7.0 Tesla MRI is required to explore white matter tracts spanning from thalamic subnuclei in patients with MDD with greater detail and accuracy.

We therefore harnessed the power of UHF dMRI at 7.0 Tesla to uniquely explore the structural connectivity of thalamic subnuclei in MDD. We hypothesized abnormal white matter connectivity of thalamic subnuclei in MDD versus HC participants, as indexed by changes in FA, AD, MD, radial diffusivity (RD), and streamline count (SLC). Additionally, we expect several clinical variables are associated with thalamic subnucleus connectivity characteristics.

2. Method

2.1. Participants

The implementation of this study should follow the approach used in our previous research (Heij et al., 2024; Liu et al., 2024a, 2024b). Patients with MDD recruited in this study met the following inclusion criteria: (1) a primary diagnosis of current MDD that occurred within the last 6 months, according to DSM-5 criteria, as determined by the Composite International Diagnostic Interview (CIDI) (Smeets and Dingemans, 1993); (2) aged between 20 and 55. HCs met the following inclusion criteria: (1) no history of depression diagnosis or treatment, nor any other psychopathology; (2) normal or subclinical scores on dimensional measures of psychopathology; (3) aged between 20 and 55. Exclusion criteria for the entire sample: (1) presence of psychoses, mania, Tourette's syndrome, or obsessive-compulsive disorder; (2) diagnosis of major internal or neurological disorders; (3) traumatic head injury; (4) current substance abuse or dependence requiring treatment; (5) evidence of acute suicidal risk requiring immediate intervention; (6) MRI contradictions, including metal implants, heart arrhythmia, or claustrophobia; (7) left-handedness; (8) pregnancy; (9) inadequate understanding of the Dutch language.

Seventy-one participants were enrolled in our study (57 patients with MDD and 14 HCs). In the MDD group, one patient was excluded because of a low quality T1 image, one patient for low quality dMRI images, and two patients for lacking dMRI images. In the HC group, one participant was excluded here for low quality dMRI images and one participant for lacking dMRI images. The final sample consisted of 53 participants with a primary diagnosis of MDD (mean age = 36.57 years, SD = 10.71 years, 40 females) and 12 HC participants (mean age = 34.37 years, SD = 9.67 years, 7 females). Detailed demographic and clinical information are shown in Table 1. The medical ethical review board of the Amsterdam UMC (location VUmc) approved this study, and written informed consent was obtained from all participants.

2.2. Clinical measures

The Inventory for Depressive Symptomatology (IDS) was used to measure the severity of depression (Rush et al., 1996). To meet the criteria for atypical MDD, patients needed to have specific scores on various IDS items. Emotional reactivity required scores of 0, 1, or 2, leaden paralysis required scores of 2 or 3, weight gain or increased appetite required scores of 2 or 3, hypersomnia required scores of 2 or 3, and interpersonal sensitivity required a score of 3. Furthermore, to be classified as having atypical MDD, patients had to be emotionally reactive (not scoring 3 on the emotional response item) and meet the criteria for at least 2 of the other 4 symptoms (Novick et al., 2005). The Beck Anxiety Inventory (BAI) was used to measure anxiety severity

Table 1Demographical and clinical information of the participants.

	MDD (n = 53)	HC (n = 12)	BF ₁₀
Age (years), mean \pm SD	36.57 ± 10.71	34.37 ± 9.67	0.368
Gender (female), n (%)	40 (75.47 %)	7 (58.33 %)	0.703
Age of onset (years) ^a , mean \pm SD	21.33 ± 10.50	-	-
Recurrent MDD, n (%)	22 (41.51 %)	_	-
With atypical MDD ^a , n (%)	14 (26.92 %)	_	-
${ m IDS}^{ m a}$, mean \pm SD	34.21 ± 13.19	$\textbf{4.08} \pm \textbf{2.81}$	7.016E7
BAI^a , mean \pm SD	14.33 ± 9.67	2.42 ± 2.35	417.837
IRS^a , mean \pm SD	9.81 ± 5.16	5.25 ± 4.43	6.851
CTQ^a , mean \pm SD	47.15 \pm	35.58 \pm	2.082
	17.78	6.78	
With any psychotropic medications, n (%)	30 (56.60 %)	-	_
With any antidepressants, n (%)	27 (50.94 %)	_	-
With SSRIs and/or SNRIs, n (%)	20 (37.74 %)	_	-
With TCA, n (%)	8 (15.09 %)	_	_
With atypical antidepressants, n (%)	2 (3.77 %)	-	_
With lithium stabilizer, n (%)	3 (5.66 %)	-	_
With antipsychotics, n (%)	6 (11.32 %)	-	_
With benzodiazepines, n (%)	6 (11.32 %)	-	-

Bold indicates moderate or greater evidence.

Abbreviation: MDD = major depressive disorder; HC = healthy control; SD = standard deviation; IDS = Inventory for Depressive Symptomatology; BAI = Becks Anxiety Inventory; IRS = Insomnia Rating Scale; CTQ = Childhood Trauma Questionnaire; SSRI = selective serotonin reuptake inhibitor; SNRI = serotonin-norepinephrine reuptake inhibitor; TCA = tricyclic antidepressant.

^a One MDD patient did not provide the age of onset, and another MDD patient did not provide data for IDS, BAI, IRS, and CTQ. Therefore, when analyzing the data related to these indicators, the sample size for MDD is 52 individuals.

(Beck et al., 1988). The Insomnia Rating Scale (IRS) was used to measure the severity of insomnia (Levine et al., 2003). The Childhood Trauma Questionnaire (CTQ) was used to measure the severity of childhood trauma (de Graaf et al., 2002).

2.3. MRI acquisition

Images were acquired using a Philips Achieva 7 T MRI scanner with a 32-channel head array coil (Liu et al., 2024b). A diffusion-weighted imaging (DWI) sequence was used with the following parameters: Echo time (TE) = 74 ms, repetition time (TR) = 11,224 ms, field of view (FOV) = $214 \times 126.5 \times 214$ mm, flip angle = 90° , spatial resolution = $1.337 \times 1.337 \times 1.49$ mm, and the number of gradient directions = 64. The b-value for the sequence was 1200 s/mm^2 , and one $b = 0 \text{ s/mm}^2$ was acquired. Additionally, two DWI reverse phase-encoding direction scans were acquired to correct for gradient distortions (Andersson and Sotiropoulos, 2016). T1 weighted images were obtained as anatomical reference using a multi-echo magnetization-prepared rapid gradient echo (MP2RAGEME) sequence (Caan et al., 2019). The MP2RAGEME is an extension of the MP2RAGE sequence (Marques et al., 2010) and consists of two rapid gradient echo (GRE1.2) images that are acquired after a 180° degrees inversion pulse and excitation pulses with inversion times $TI_{1,2} = [670 \text{ ms}, 3675.4 \text{ ms}]$. A multi-echo readout was used in the second inversion, with four equally spaced echo times ($TE_1 = 3$ ms, $TE_{2,1-4} = 3$, 11.5, 19, 28.5 ms). Other scan parameters include flip $angle_{1,2} = [4^{\circ}, 4^{\circ}]; TR_{GRE1,2} = [6.2 \text{ ms}, 31 \text{ ms}]; bandwidth = 404.9 \text{ MHz};$ $TR_{MP2RAGEME} = 6778$ ms; acceleration factor $SENSE_{PA} = 2$; FOV = 205 \times 205 \times 164 mm; acquired voxel size = 0.7 \times 0.7 \times 0.7 mm; acquisition matrix was 292 \times 290; reconstructed voxel size 0.64 \times 0.64 \times 0.7 mm; turbo factor (TFE) = 150, resulting in 176 shots; Total acquisition time = 19.53 min.

2.4. Thalamic segmentation

The T1-weighted images were preprocessed using the "recon-all" pipeline with FreeSurfer version 7.2.0 (http://surfer.nmr.mgh.harvard.edu). The preprocessing steps include normalization of signal intensity, skull stripping, talairach correction, and automated segmentation of subcortical white matter and grey matter structures (Fischl, 2012).

Afterwards, the preprocessed T1-weighted images were subjected to thalamic segmentation using FreeSurfer's subregion segmentation module, which demonstrated excellent test-retest reliability and remained robust to variations in input MRI contrast (Iglesias et al., 2018). In this step, a probabilistic atlas constructed from histological data using Bayesian inference was employed to segment the thalamus into 25 different nuclei: anteroventral nucleus (AV), laterodorsal nucleus (LD), lateral posterior nucleus (LP), ventral anterior nucleus (VA), ventral anterior magnocellular nucleus (VAmc), ventral lateral anterior nucleus (VLa), ventral lateral posterior nucleus (VLp), ventral posterolateral nucleus (VPL), ventromedial nucleus (VM), centromedian nucleus (CM), central medial nucleus (CeM), central lateral nucleus (CL), paracentral nucleus (Pc), parafascicular nucleus (Pf), paratenial nucleus (Pt), reuniens (medial ventral) nucleus (MV-re), mediodorsal medial magnocellular nucleus (MDm), mediodorsal lateral parvocellular nucleus (MDl), lateral geniculate nucleus (LGN), medial geniculate nucleus (MGN), limitans (suprageniculate) nucleus (L-SG), pulvinar anterior nucleus (PuA), pulvinar medial nucleus (PuM), pulvinar lateral nucleus (PuL), and pulvinar inferior nucleus (PuI).

According to Krauth's atlas, which extensively characterizes functional and structural thalamic connectivity, we combined LD and LP lateral posterior to form the lateral nucleus (LTR), while CM, CeM, CL, Pc, and Pf were classified as the intralaminar nucleus (ITL). Similarly, Pt, MV-re, MDm, and MDl were designated as the medial nucleus (MED) (Iglesias et al., 2018; Krauth et al., 2010). Additionally, VM, VAmc, and PuA were excluded from the analysis because fewer than two-thirds of individuals produced any streamlines spanning from these regions. Fig. 1A-C shows all thalamic subnuclei that ended up in the final tractography. Segmentations were inspected manually.

2.5. Diffusion data preprocessing

Diffusion data were processed with MRtrix version 3.0.4 and FSL version 6.0.5.2. The diffusion images were subjected to denoising and Gibbs ringing removal using MRtrix (Cordero-Grande et al., 2019; Kellner et al., 2016; Veraart et al., 2016a, 2016b). FSL was employed for correcting susceptibility-induced distortions, eddy currents, and motion artifacts (Andersson et al., 2003; Andersson and Sotiropoulos, 2016; Smith et al., 2004). Additionally, DWI images were corrected for field inhomogeneities using ANTs' N4 bias correction (Tustison et al., 2010). Next, the corrected diffusion-weighted images were co-registered to T1w space using FSL-FLIRT (Jenkinson et al., 2002; Jenkinson and Smith, 2001). MRtrix was utilized to generate a segmented tissue image, along with a mask image suitable for seeding streamlines at the grey matter-white matter interface (Smith et al., 2012). The estimation of the diffusion tensor was performed based on weighted least-squares (Basser et al., 1994a; Veraart et al., 2013), while the response function was estimated for constrained spherical deconvolution (Tournier et al., 2019). We employed constrained spherical deconvolution to estimate fiber orientation distributions (FOD) from the diffusion data (Jeurissen et al., 2014). For microstructure analysis of DTI measures, we locally fitted the diffusion tensor in each voxel, resulting in whole-brain maps encompassing FA (a diffusion coherence index), AD (diffusion magnitude in the primary direction), MD (the total diffusion magnitude averaged across measured directions), and RD (the averaged diffusion magnitude in orthogonal secondary and tertiary directions) (Basser et al., 1994b). A schematic representation of key DTI indices and their properties is shown in Supplemental Fig. 1 (Heij et al., 2019).

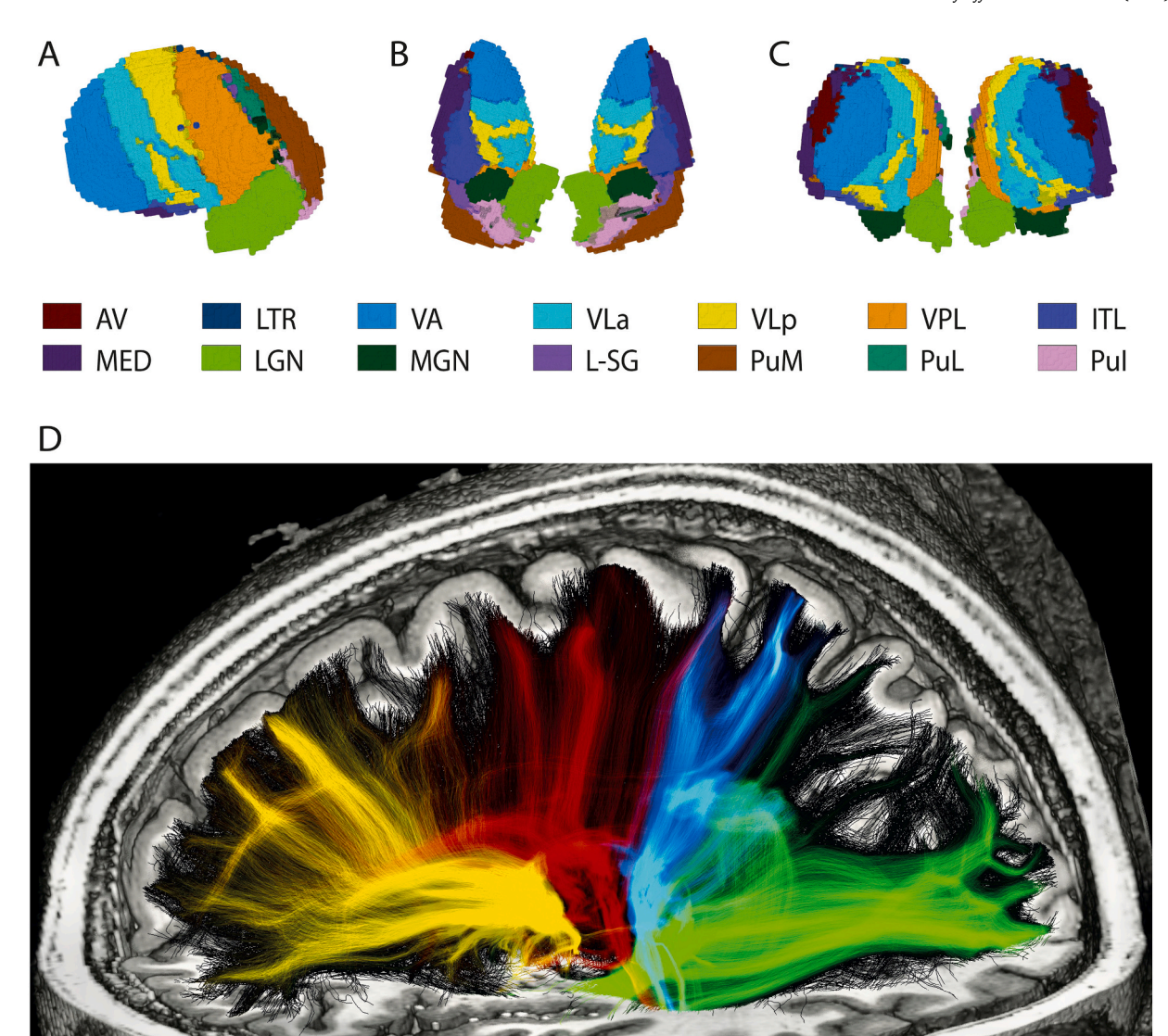


Fig. 1. All thalamic subnuclei in the final tractography and thalamocortical main radiations.

A-C: Figures are arranged in the order of sagittal, axial, and coronal views. Abbreviation: AV = anteroventral nucleus; LTR = lateral nucleus; VA = ventral anterior nucleus; VLa = ventral lateral anterior nucleus; VLp = ventral lateral posterior nucleus; VPL = ventral posterolateral nucleus; ITL = intralaminar nucleus; MED = medial nucleus; LGN = lateral geniculate nucleus; MGN = medial geniculate nucleus; L-SG = limitans (suprageniculate) nucleus; PuM = pulvinar medial nucleus; PuL = pulvinar lateral nucleus; PuI = pulvinar inferior nucleus.

D: Colour coding: yellow, prefrontal; red, precentral-premotor; blue, postcentral-precuneus; green, parieto-occipital. (For interpretation of the references to colour in this figure legend, the reader is referred to the web version of this article.)

2.6. Tractography

Probabilistic tractography was performed using MRtrix (Smith et al., 2012; Tournier et al., 2010). Each thalamic subnucleus mask was used as an individual seed region (Fig. 1A-C), with 200,000 random seeds initiated. Streamline generation was limited to the ipsilateral hemisphere from each thalamic subnucleus, excluding the remaining thalamus subnuclei to prevent tract overlap. To control streamline generation, we applied a threshold by setting an FOD amplitude cutoff of 0.05 and limiting the maximum angle between successive streamline generation steps to 60° . Due to the close proximity of the MGN to the LGN, which primarily projects to the visual cortex (Keifer et al., 2015), when performing tractography on the corresponding fibers of the MGN, we excluded the visual cortex. From each voxel along every streamline,

microstructural measurements including FA, MD, RD, and AD were extracted. The mean measurements per streamline were computed and subsequently averaged to obtain a single mean value for FA, MD, RD, and AD per participant within each thalamic subnucleus ROI (Smith et al., 2013). The spherical deconvolution (SIFT2) algorithm was applied to all tracts. Its purpose was to optimize per-streamline cross-section multipliers in order to match the whole-brain tractogram with fixel-wise fiber densities (Smith et al., 2015). The extraction of SLC incorporated SIFT2 weightings to improve accuracy with respect to ground truth white matter and to remove spurious streamlines.

2.7. Statistical analysis

For basic demographic and clinical data comparisons, the Bayesian

chi-square test was used for dichotomous variables and the Bayesian independent samples t-test for continuous variables as implemented in JASP (version 0.17.1: https://jasp-stats.org/) (van Doorn et al., 2021). The Bayesian factor (BF) was interpreted using the following evidence categories: BF < 3 (and its reciprocal) indicates anecdotal evidence for Hypothesis 1; BF \geq 3 corresponds to moderate evidence; BF \geq 10 suggests strong evidence; BF \geq 30 represents very strong evidence; and BF > 100 indicates extreme evidence (Lee and Wagenmakers, 2014).

The Bayesian multilevel (BML) model was conducted to investigate the strength of the differences in white matter metrics between MDD and HC and the relationship between white matter metrics and clinical features through the AFNI program region-based analysis (RBA) with 4 Markov chains each of which had 1000 iterations in R (version 4.4.0: https://cran.r-project.org/) (Chen, 2022; Chen et al., 2020, 2019b). Five DTI metrics (FA, MD, RD, AD and SLC) were included in the BML. Unlike traditional null hypothesis significance testing (NHST), the BML model overcomes inefficiencies and over-penalties in current large-scale univariate methods and corrects for multiple testing, making it more efficient (Chen et al., 2019b). We replaced standard significance testing with inferring the credibility of evidence from posterior distributions (Liu et al., 2022): moderate evidence is indicated by a positive posterior probability (P+) of <0.10 or >0.90, strong evidence by a P+ of <0.05 or >0.95, and very strong evidence by a P+ of <0.025 or >0.975 (Chen et al., 2019a).

Our primary focus was on the group effect (MDD/HC). Results with moderate or stronger evidence (P+>0.90) were incorporated into the further analyses which examined clinical factors (medicated/non-medicated MDD, typical/atypical MDD, first episode/recurrent MDD, age of onset, and scores of the IDS, BAI, IRS, and CTQ). To control for confounding variables, age, gender, and ICV were also included in each analysis. In this study, we presented results with all levels of evidence and focused on results with strong evidence.

3. Results

3.1. Demographical and clinical features

A total of 53 MDD patients and 12 HCs were enrolled in the present study (see Table 1). The MDD group comprised 40 females (75.47 %), while the HC group included 7 females (58.33 %). Among the MDD patients, 22 individuals had recurrent depression (41.51 %), with a mean age of onset of 21.33 ± 10.50 years. The Bayesian independent samples t-test and the Bayesian chi-square test provided no evidence that age, gender, and scores of CTQ were different between the MDD group and HC group (all BF $_{10}$ < 3). Moderate or greater evidence was found suggesting that MDD patients have higher scores of IDS, BAI, and IRS (all BF $_{10}$ < 3). Demographical and clinical details are shown in Table 1.

3.2. Qualitative description of thalamic subnuclear anatomical connections

As shown in Fig. 1D, we reproduced the four main bundles of the thalamocortical projection system: yellow, prefrontal; red, precentral motor; blue, postcentral precuneus; green, parieto-occipital, which indicated that we get a good quality of tractography. Each bundle of each subject was visually inspected to ensure the accuracy of fiber tracking. All tracts essentially project into regions reported in previous literature or anatomical evidence (Fig. 2A-N). Detailed quantitative information on white matter indicators is shown in Supplementary Tables 1–5.

$3.3.\,\,$ MDD participants have lower thalamic white matter metrics than HC participants

MDD participants had lower thalamic subnucleus white matter

metrics than HC participants for all the included measures (Supplemental Fig. 2). Moderate to strong evidence (P+>0.90) showed that differences in white matter metrics between MDD participants and HCs involved all (14) thalamic subnuclei (Fig. 3A).

The BML model showed strong evidence of lower SLC of tracts spanning from left PuM (P+=0.9715, Fig. 3B), FA of tracts spanning from right LTR (P+=0.9710, Fig. 3C), FA of tracts spanning from bilateral VA (left: P+=0.9660, Fig. 3D; right: P+=0.9695, Fig. 3E), FA of tracts spanning from right AV (P+=0.9670, Fig. 3F), FA of tracts spanning from right ITL (P+=0.9600, Fig. 3G), RD and MD of tracts spanning from bilateral PuI (left-RD: P+=0.9570, Fig. 3H; left-MD: P+=0.9565, Fig. 3I; right-RD: P+=0.9515, Fig. 3J; right-MD: P+=0.9520, Fig. 3K), FA of tracts spanning from left VPL (P+=0.9525, Fig. 3L), and FA of tracts spanning from left MGN (P+=0.9510, Fig. 3M) in MDD patients compared to HCs.

3.4. Medication is related to higher white matter metrics in MDD

For the medication status, medicated MDD participants showed moderate evidence of higher AD of tracts spanning from right Vla (P+ = 0.0995, Fig. 4).

3.5. Later onset is related to higher white matter metrics in MDD

Fig. 5A showed the evidence of a positive correlation between age of onset and white matter metrics of thalamic subnuclei. Strong evidence revealed that age of onset is positively associated with AD of tracts spanning from bilateral LGN (left: P+=0.9720, Fig. 5B; right: P+=0.9690, Fig. 5C), AD of tract spanning from bilateral ITL (left: P+=0.9520, Fig. 5D; right: P+=0.9690, Fig. 5E), AD of tract spanning from bilateral MGN (left: P+=0.9690, Fig. 5F; right: P+=0.9685, Fig. 5G), MD of tract spanning from right LGN (P+=0.9675, Fig. 5H), AD of tract spanning from left VPL (P+=0.9665, Fig. 5J), AD and MD of tract spanning from left VIa (AD: P+=0.9635, Fig. 5J; MD: P+=0.9565, Fig. 5K), FA of tract spanning from left ITL (P+=0.9630, Fig. 5L), FA of tract spanning from left PuM (P+=0.9610, Fig. 5M), RD and SLC of tract spanning from left L-SG (RD: P+=0.9565, Fig. 5N; SLC: P+=0.9525, Fig. 5O), and FA of tract spanning from left MED (P+=0.9525, Fig. 5P).

3.6. Recurrence is related to higher white matter metrics in MDD

For the recurrence, recurrent MDD participants showed moderate evidence of higher white matter metrics involving most of the thalamic subnuclei (except the LTR, all P+<0.10) compared to first episode MDD participants (Fig. 6).

Furthermore, the current study did not find moderate or above evidence that the white matter metrics of thalamic subnuclei were associated with the typical type of MDD, and scores of IDS, BAI, IRS, and CTQ in participants with MDD (Supplemental Figs. 3–7. $0.10 \le \text{all } P+ \le 0.90$).

4. Discussion

This study represents the first investigation into the structural connectivity of thalamic subnuclei in patients with MDD, using UHF dMRI at 7.0 Tesla. Prior work on thalamic white matter connectivity has almost exclusively employed standard field strength MRI (1.5/3.0 Tesla), probing the thalamus as a whole and overlooking its subnuclear composition. Harnessing the power of UHF dMRI, allowing subnuclear examination of the thalamus, we identified certain white matter structural connectivity abnormalities that have not been identified by previous studies. Specifically, we find that MDD and clinical characteristics (medication status, age of onset and recurrence) relate to altered thalamic subnuclear connectivity with cortical and subcortical circuits governing sensory processing, emotional function, and goal-directed

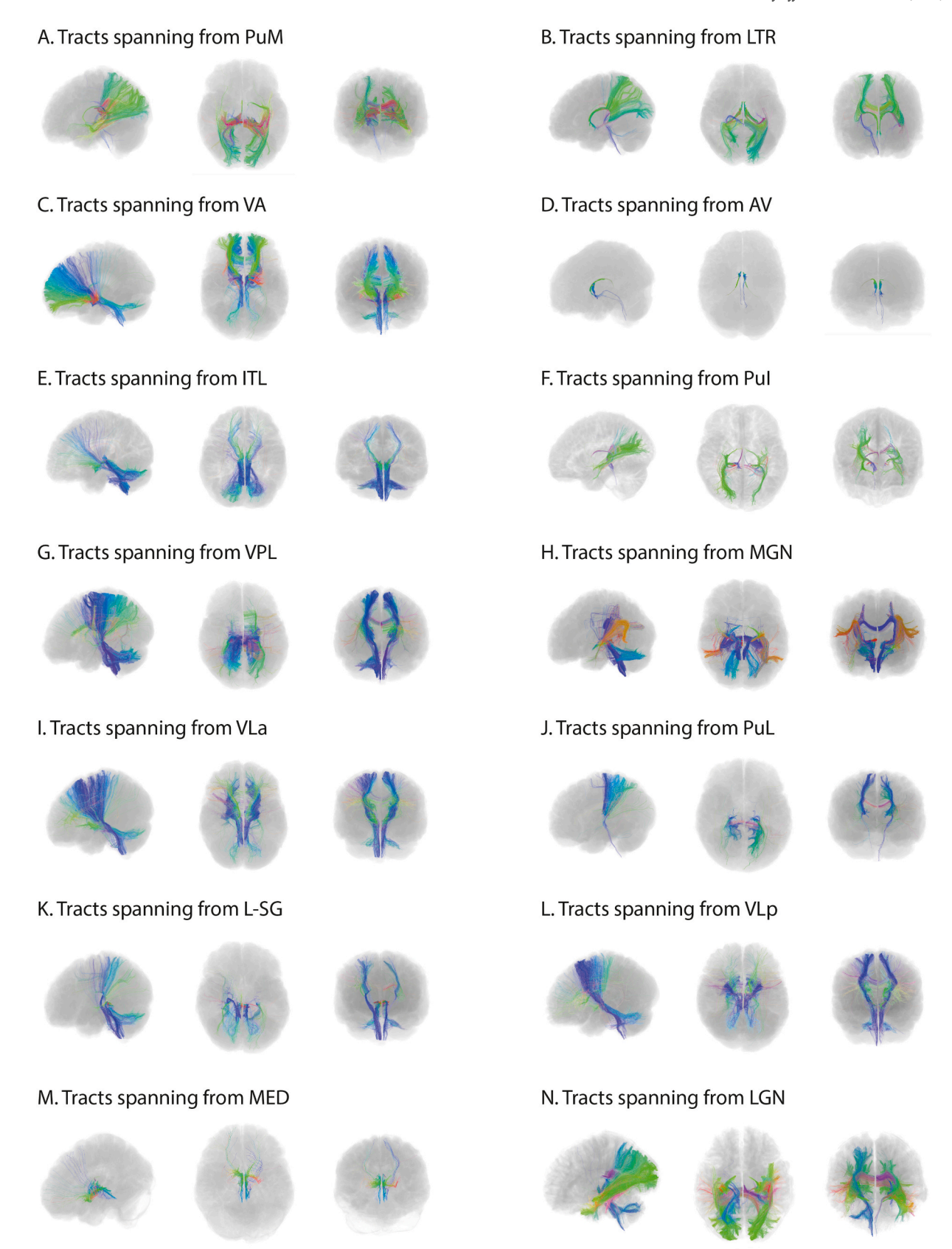


Fig. 2. All thalamic subnuclei tracts.

Figures are arranged in the order of sagittal, axial, and coronal views. Abbreviation: AV = anteroventral nucleus; LTR = lateral nucleus; VA = ventral anterior nucleus; VLa = ventral lateral anterior nucleus; VLp = ventral lateral posterior nucleus; VPL = ventral posterolateral nucleus; ITL = intralaminar nucleus; MED = medial nucleus; LGN = lateral geniculate nucleus; MGN = medial geniculate nucleus; L-SG = limitans (suprageniculate) nucleus; PuM = pulvinar medial nucleus; PuL = pulvinar lateral nucleus; PuI = pulvinar inferior nucleus.

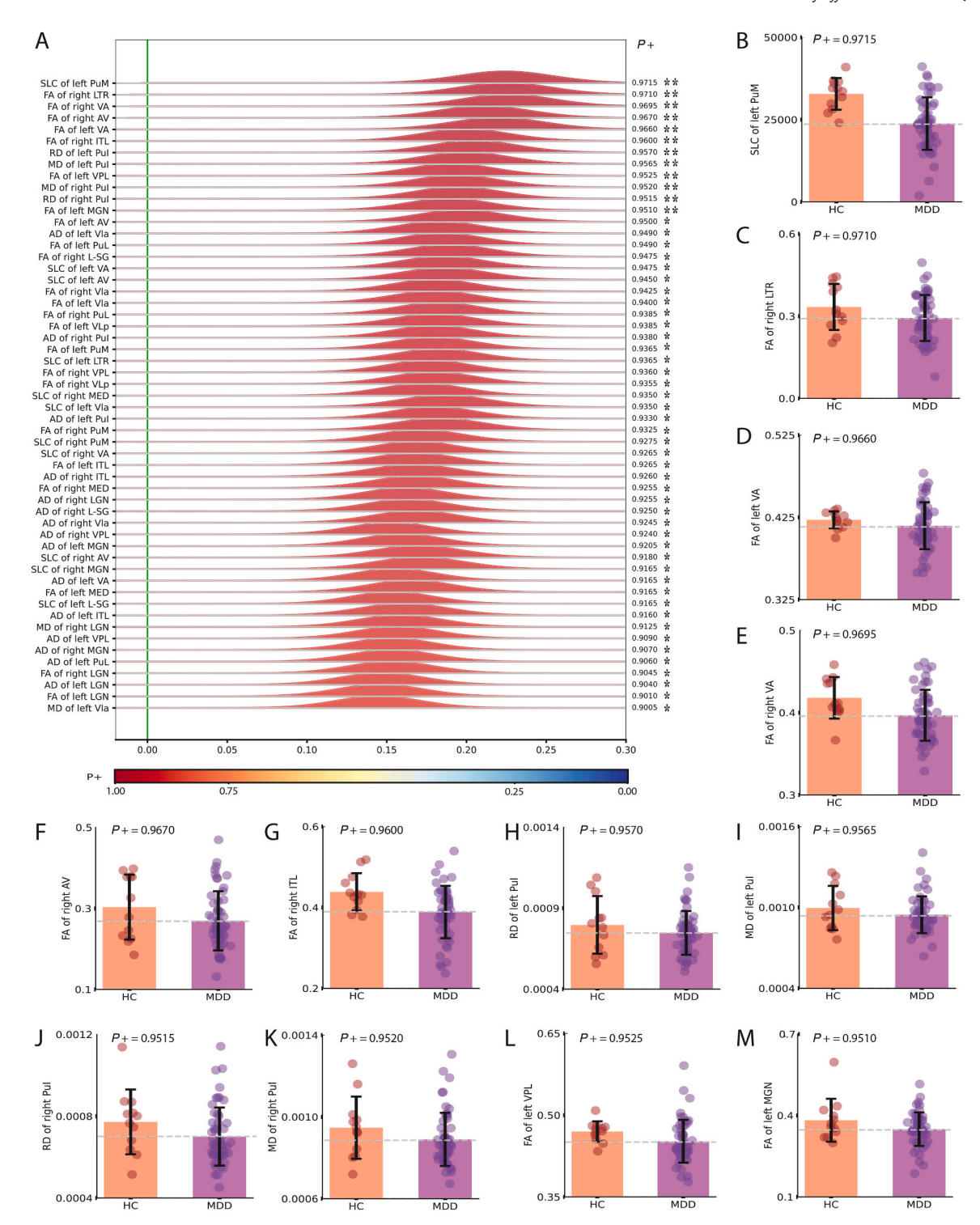


Fig. 3. Comparisons of white matter metrics with moderate and above evidence between MDD and HC.

A: Posterior distribution of the effect (HC versus MDD) in each white matter metric with moderate and above evidence (P > 0.90). Hue indicates the strength of statistical evidence according to the Bayesian multilevel model, shown through P + 0.90. The x-axis is the effect of each white matter metric (in Fisher's z-value). The vertical green line indicates zero effect. Metrics with relatively strong evidence of the valence effect can be identified as the extent of the green line being farther into the tail of the posterior distribution.

Abbreviation: FA = fractional anisotropy; AD = axial diffusivity; MD = mean diffusivity; RD = radial diffusivity; SLC = streamline count; AV = anteroventral nucleus; LTR = lateral nucleus; VA = ventral anterior nucleus; VLa = ventral lateral anterior nucleus; VLp = ventral lateral posterior nucleus; VPL = ventral posterolateral nucleus; ITL = intralaminar nucleus; MED = medial nucleus; LGN = lateral geniculate nucleus; MGN = medial geniculate nucleus; L-SG = limitans (suprageniculate) nucleus; PuM = pulvinar medial nucleus; PuL = pulvinar lateral nucleus; PuI = pulvinar inferior nucleus. (For interpretation of the references to colour in this figure legend, the reader is referred to the web version of this article.)

^{*:} Moderate evidence (P+<0.10 or >0.90).

^{**:} Strong evidence (P+ < 0.05 or >0.95).

B-M: Bar charts of every thalamic white matter with strong evidence (P+>0.95).

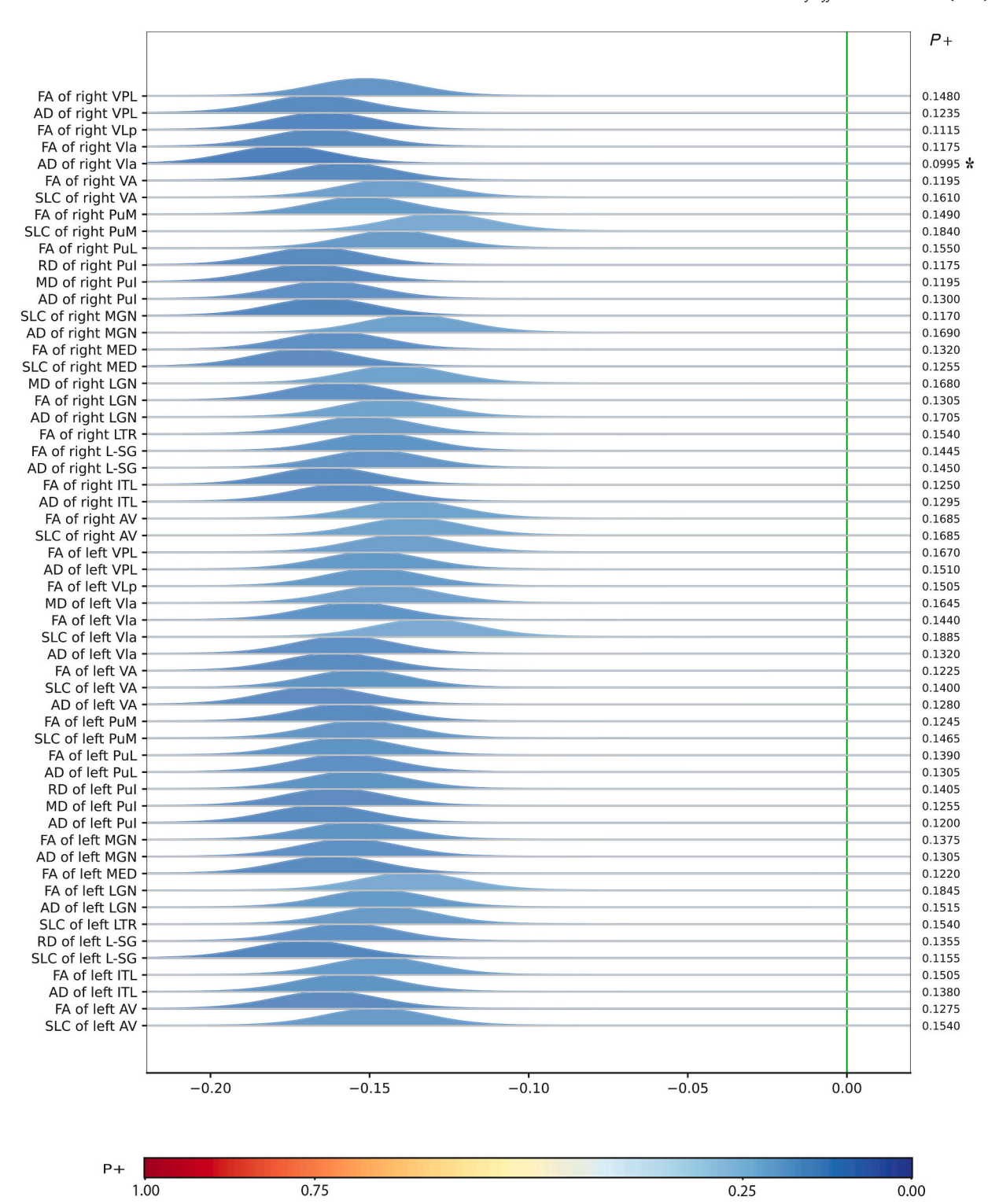


Fig. 4. Comparisons of white matter metrics with moderate evidence between medicated and non-medicated MDD. Posterior distribution of the effect (medicated versus non-medicated MDD) in each white matter metric with moderate and above evidence (P+>0.90). Hue indicates the strength of statistical evidence according to the Bayesian multilevel model, shown through P+. The x-axis is the effect of each white matter metric (in Fisher's z-value). The vertical green line indicates zero effect. Metrics with relatively strong evidence of the valence effect can be identified as the extent of the green line being farther into the tail of the posterior distribution.

*: Moderate evidence (P+ < 0.10 or > 0.90).

Abbreviation: FA = fractional anisotropy; AD = axial diffusivity; MD = mean diffusivity; RD = radial diffusivity; SLC = streamline count; AV = anteroventral nucleus; LTR = lateral nucleus; VA = ventral anterior nucleus; VLa = ventral lateral anterior nucleus; VLp = ventral lateral posterior nucleus; VPL = ventral posterolateral nucleus; ITL = intralaminar nucleus; MED = medial nucleus; LGN = lateral geniculate nucleus; MGN = medial geniculate nucleus; L-SG = limitans (suprageniculate) nucleus; PuM = pulvinar medial nucleus; PuL = pulvinar lateral nucleus; PuI = pulvinar inferior nucleus. (For interpretation of the references to colour in this figure legend, the reader is referred to the web version of this article.)

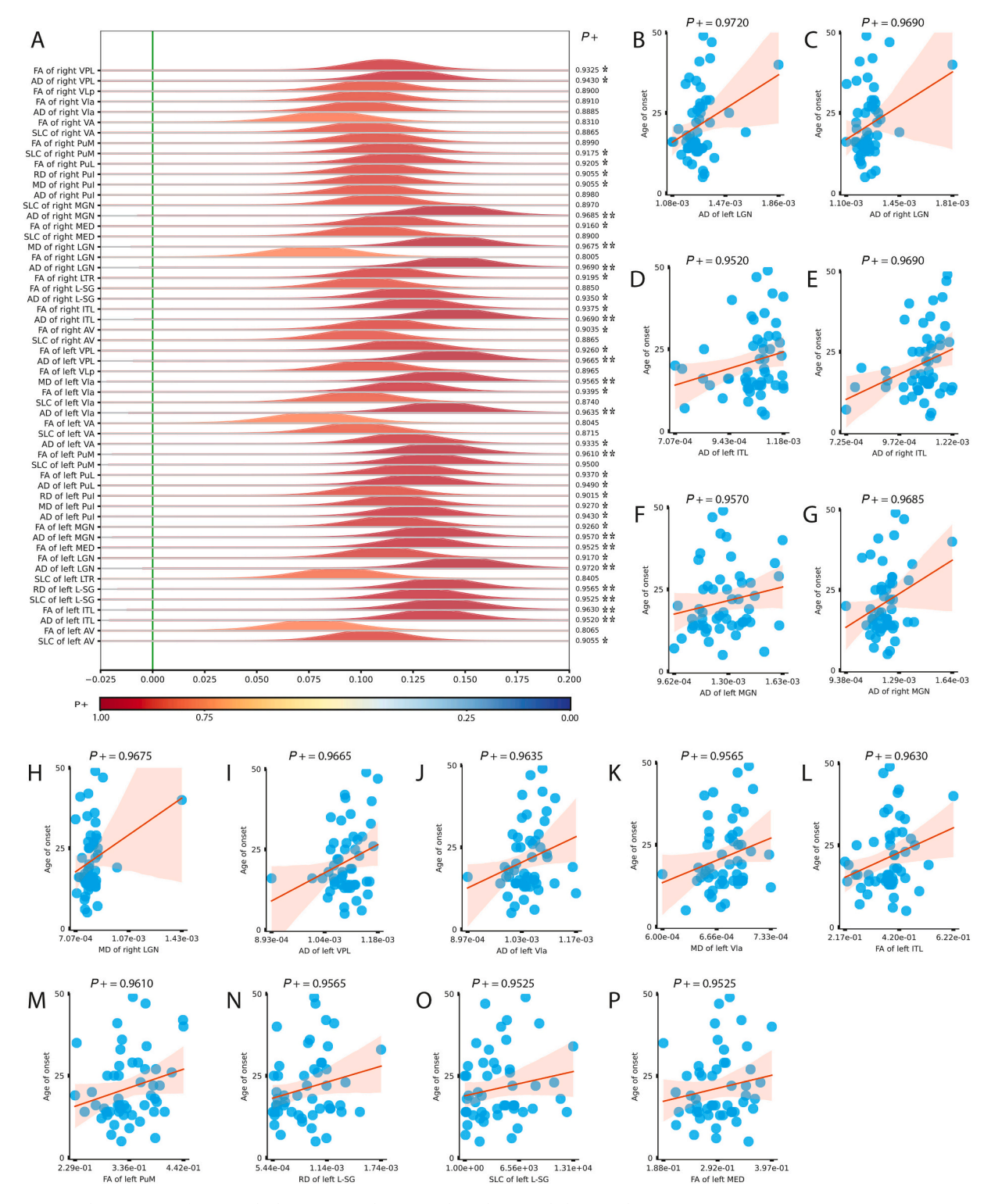


Fig. 5. Association between age of onset and white matter indicators with moderate and above evidence in MDD. A: Posterior distribution of the effect (age of onset) in each white matter metric. Hue indicates the strength of statistical evidence according to the Bayesian multilevel model, shown through P+. The x-axis is the effect of each white matter metric (in Fisher's z-value). The vertical green line indicates zero effect. Metrics with relatively strong evidence of the valence effect can be identified as the extent of the green line being farther into the tail of the posterior distribution. *: Moderate evidence (P+ < 0.10 or > 0.90).

B-P: Scatter plots of every thalamic white matter with P+ > 0.95.

Abbreviation: FA = fractional anisotropy; AD = axial diffusivity; MD = mean diffusivity; RD = radial diffusivity; SLC = streamline count; AV = anteroventral nucleus; LTR = lateral nucleus; VA = ventral anterior nucleus; VLa = ventral lateral anterior nucleus; VLp = ventral lateral posterior nucleus; VPL = ventral posterior nucleu nucleus; ITL = intralaminar nucleus; MED = medial nucleus; LGN = lateral geniculate nucleus; MGN = medial geniculate nucleus; L-SG = limitans (suprageniculate) nucleus; PuM = pulvinar medial nucleus; PuL = pulvinar lateral nucleus; PuI = pulvinar inferior nucleus. (For interpretation of the references to colour in this figure legend, the reader is referred to the web version of this article.)

^{**:} Strong evidence (P+ < 0.05 or > 0.95).

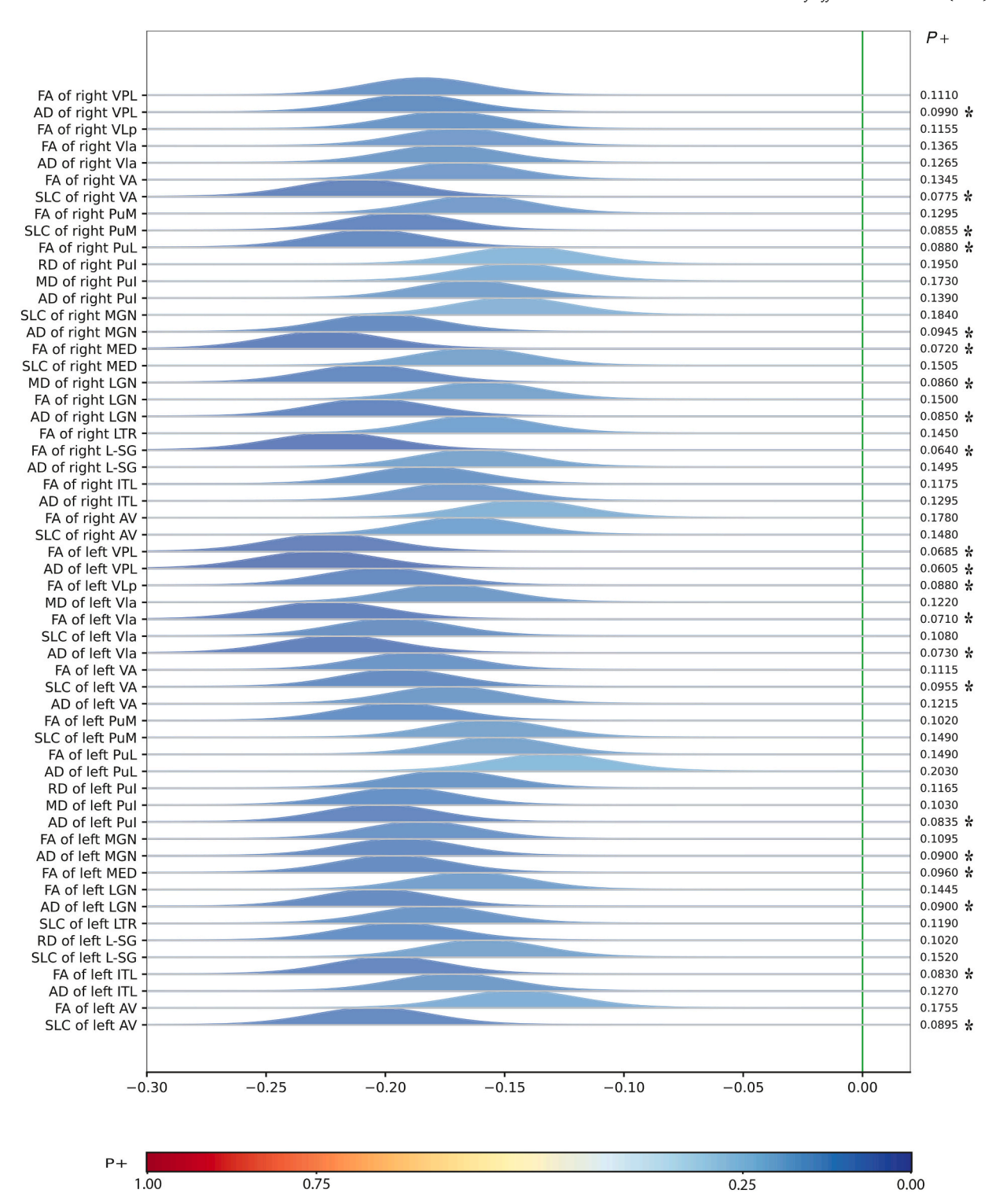


Fig. 6. Comparisons of white matter metrics with moderate evidence between first episode and recurrent MDD. Posterior distribution of the effect (first episode versus recurrent MDD) in each white matter metric with moderate and above evidence (P+>0.90). Hue indicates the strength of statistical evidence according to the Bayesian multilevel model, shown through P+. The x-axis is the effect of each white matter metric (in Fisher's z-value). The vertical green line indicates zero effect. Metrics with relatively strong evidence of the valence effect can be identified as the extent of the green line being farther into the tail of the posterior distribution.

Abbreviation: FA = fractional anisotropy; AD = axial diffusivity; MD = mean diffusivity; RD = radial diffusivity; SLC = streamline count; AV = anteroventral nucleus; LTR = lateral nucleus; VA = ventral anterior nucleus; VLa = ventral lateral anterior nucleus; VLp = ventral lateral posterior nucleus; VPL = ventral posterolateral nucleus; ITL = intralaminar nucleus; MED = medial nucleus; LGN = lateral geniculate nucleus; MGN = medial geniculate nucleus; L-SG = limitans (suprageniculate) nucleus; PuM = pulvinar medial nucleus; PuL = pulvinar lateral nucleus; PuI = pulvinar inferior nucleus. (For interpretation of the references to colour in this figure legend, the reader is referred to the web version of this article.)

^{*:} Moderate evidence (P+ < 0.10 or > 0.90).

behavior. These findings allow uniquely fine-grained insights into thalamic subnuclear structural connectivity in MDD, and cautiously implicate its involvement in the clinical manifestation of MDD.

4.1. Posterior thalamic connectivity in MDD

The current study found that white matter connections in all posterior thalamic subnuclei (except PuA, which is excluded in the current study) are different between MDD and HC, and these differences are associated with age of onset and recurrence. Our findings highlight the significant involvement of the pulvinar in MDD and clinical characteristics. SLC of left PuM showed the strongest evidence in the comparison of MDD and HC. Moreover, PuI and PuL are involved in the white matter abnormalities in MDD participants to varying degrees.

The pulvinar, as investigated in pharmacological imaging studies of thalamic neurotransmission, is a site of serotonergic and noradrenergic activity (Oke et al., 1997; Takano et al., 2008). A postmortem study involving individuals with a history of MDD reported abnormalities in the serotonin transporter system and pulvinar volume size, as determined through neuron counts (Young et al., 2007). MDD moreover seems characterized by aberrant causal interactions between the pulvinar and multiple systems, including the default mode and posterior insular networks, with the additional finding that antidepressant therapy can potentially correct or overcompensate for the pathological network behavior of the pulvinar (Hamilton et al., 2012). Recent metaanalytical examination of resting-state PET and SPECT findings in MDD also suggests that heightened baseline activity in the pulvinar contributes to an amplified response of the salience network to negative information (Tadayonnejad et al., 2016). Despite the increasing evidence of pulvinar involvement in MDD, the white matter connectional characteristics of the pulvinar in MDD have remained largely uncharted. One of the few studies on this topic shows that depression scores in patients with Parkinson's disease are associated with diminished white matter microstructure of pulvinar tracts, independent of cognitive function deficit (Bhome et al., 2022). Taken as a whole, pulvinar white matter connectional shifts as reported here, might potentially offset neurotransmitter levels and critical network function, fueling maladaptive and depressive behaviors.

Further, we found evidence that LGN tracts play a certain role in MDD. Functional circuits related to the LGN seem to be involved in the antidepressant effects of light therapy. The MGN projects to the auditory cortex (Boelens Keun et al., 2021; Huang et al., 2019). Abnormal responses in the auditory cortex are involved in the pathological mechanism of MDD (Manjarrez et al., 2011). The thalamus-primary auditory cortex circuit is a potential target for MDD treatment (Tan and Ye, 2023). In addition, our study first revealed the involvement of L-SG in MDD. There is currently no direct evidence that L-SG is associated with depression, but we found its association with MDD under ultra-high field MRI

4.2. Ventral thalamic connectivity in MDD

In addition to the pulvinar, the ventral thalamic nucleus is also recognized as a crucial brain region in depression, and our study revealed abundant evidence of abnormalities in white matter tracts connected to the ventral nucleus.

The VA receives fiber input from the substantia nigra and globus pallidus and projects to the prefrontal cortex and cingulate cortex (Boelens Keun et al., 2021). The globus pallidus is part of the striatum. The striatum and substantia nigra form the nigrostriatal pathway, which is one of the most important dopamine pathways in the brain (Klein et al., 2019). As an important part of the pathological mechanism hypothesis of MDD (Dailly et al., 2004; Tamura et al., 2022), the dopamine hypothesis is most relevant to the anhedonia symptoms of MDD (Belujon and Grace, 2017). The striatum is associated with emotion regulation (Koolschijn et al., 2009). A higher risk of depression is associated with

greater striatal connectivity within the reward network and increased striatal node strength (Pan et al., 2022, 2017). The prefrontal cortex is one of the most severely affected areas in MDD (Hare and Duman, 2020; Pizzagalli and Roberts, 2022), showing both structural and functional abnormalities in patients with MDD (Grieve et al., 2013; Murrough et al., 2016). In addition, patients with MDD have increased functional connectivity in the cingulate cortex and orbitofrontal cortex (Cheng et al., 2018). The activity level of the cingulate cortex predicts the treatment effect of MDD (Godlewska et al., 2018). Although the VA is connected to brain regions closely associated with MDD, there has been no direct evidence linking VA-related white matter to MDD, possibly due to the lower resolution of conventional MRI.

For other ventral subnuclei, the related study is relatively scarce. In a previous study, it was demonstrated that remitted MDD patients exhibited a significant reduction in grey matter volume of the right VLa, which correlated inversely with the severity of depressive symptoms (Xiong et al., 2021). Another study also found Smaller left VLp in MDD participants than HCs (Chibaatar et al., 2023). However, there are currently no reports on the relationship between VPL and MDD. Our study confirms that white matter changes originating from the ventral nucleus of the thalamus are involved in the occurrence and development of MDD, filling the gap in previous research.

4.3. Anterior thalamic connectivity in MDD

The anterior thalamic nuclei are closely associated with emotion regulation (Sun et al., 2015; Zhang et al., 2018). Stimulating the anterior thalamic nuclei can directly influence human emotions and cognitive processes (Hartikainen et al., 2014). Lower FA of bilateral AV was found in MDD participants compared to HCs in the present study. The anterior nuclei project to the hippocampus, contributing to hippocampal plasticity and episodic memory (Boelens Keun et al., 2021). Numerous studies have shown that hippocampal abnormalities are a pathological feature of MDD (Otte et al., 2016; Zhang et al., 2018), while episodic memory deficits are considered a cognitive characteristic of MDD (Dere et al., 2010). Reduced FA of the AV in MDD may contribute to mood dysregulation, making it a potential target for diagnostic evaluation and treatment.

4.4. Intralaminar thalamic connectivity in MDD

We also found evidence that lower FA within ITL tracts across MDD patients, along with higher FA within ITL tracts is related to recurrence and age of onset among MDD patients. The ITL is considered a vital relay station for a nonspecific arousal system (Steriade and Glenn, 1982). Consistently heightened brain arousal and its excessively stable regulation are considered key pathogenic factors in MDD (Schmidt et al., 2017). Sleep and arousal disturbances are common in individuals with depression, often contributing to the prominent symptom of fatigue (Surova et al., 2021). Antidepressant responders demonstrate increased levels of brain wakefulness, suggesting that dysregulation of brain arousal may serve as a predictive marker for treatment response in depression (Schmidt et al., 2017). The ITL is involved in higher-order cognitive processes, and damage to ITL can impair non-hippocampaldependent working memory tasks (Vertes et al., 2022). Cognitive impairment is also a prominent feature among individuals with MDD (Otte et al., 2016). Furthermore, there is evidence indicating a negative correlation between the volume of the ITL and anxious arousal (Casteen et al., 2022). Our finding suggests that the abnormality of ITL tracts might be related to the onset and recurrence of MDD.

4.5. Lateral thalamic connectivity in MDD

Evidence was found for lower FA within right LTR tracts among MDD patients, and the FA of right LTR is positively associated with the age of onset. Previous studies have found that the lateral nuclear volume of

MDD patients is smaller than that of HCs (Chibaatar et al., 2023). Furthermore, the LTR is involved in limbic function (Boelens Keun et al., 2021), which is related to motivational behavior and emotion (Spellman and Liston, 2020). The limbic system is involved in the occurrence and development of MDD (Mayberg et al., 1999; Milaneschi et al., 2019). Our study demonstrates for the first time LTR-related white matter abnormalities that are closely related to limbic function in MDD patients.

4.6. Medial thalamic connectivity in MDD

Moderate evidence suggests that MDD patients have lower white matter indices within the MED tract than HCs and that these white matter indices are associated with the age of onset and recurrence in MDD participants. The MED of the thalamus projects to the amygdala and hippocampus and exhibits strong interconnections with the prefrontal cortex (Boelens Keun et al., 2021). These regions are highly implicated in depression and anxiety, and the MED is involved in emotional processing (Mitchell and Gaffan, 2008; Ouhaz et al., 2018). These findings suggest that the MED connections play a certain role in aspects of MDD.

Additionally, opposing white matter differences were found in recurrent vs. first episode MDD patients with respect to MDD vs. HC. Recurrent MDD patients may exhibit neuroplasticity or compensatory white matter changes after repeated depressive episodes (De Marco et al., 2017). This can manifest as increased white matter indices in the thalamus, reflecting attempts to adapt or reorganize brain connections. Although there were no differences in demographics and use of medications between recurrent and first episode MDD (supplemental table 6), recurrent MDD patients may have undergone long-term treatments. Some studies suggest that antidepressants may promote myelination or enhance white matter integrity (Pittenger and Duman, 2008; van Velzen et al., 2020; Wang et al., 2023). This may have contributed to the relatively higher white matter metrics in recurrent MDD patients.

4.7. Strengths and limitations

We used higher spatial resolutions (approximately 3-fold $(1.4^3 \, \mathrm{mm}^3)$ vs. $2.0^3 \, \mathrm{mm}^3$)) to explore the characteristics of thalamic subnuclei structural connectivity in MDD. The cross-sectional nature of the study precludes firm conclusions regarding causality, making it difficult to dissect whether reported white matter anomalies are a cause or consequence of MDD. Due to the financial burden and time constraints at play when conducting UHF MRI research, we chose to maximize and prioritize the inclusion of our main target group (MDD), which resulted in a relatively small HC sample. That said, the 53 MDD patients included here render this the largest UHF dMRI examination of the thalamic subnuclei in MDD to date, and the use of Bayesian statistics mitigates the risk of biased results with small samples (van de Schoot et al., 2014).

5. Conclusions

By harnessing the power of UHF dMRI at 7.0 Tesla for subnuclear examination of the thalamus, we found certain white matter connectivity abnormalities in MDD patients, and these white matter abnormalities were associated with clinical features, which have not been identified with standard dMRI. This includes altered connectivity of thalamic subnuclei with cortical and subcortical circuits that govern sensory processing, emotional function, and goal-directed behavior. These findings fill critical knowledge gaps, by allowing uniquely finegrained insights on thalamic subnuclear connectivity shifts that may underpin the clinical manifestation of MDD. Future work should examine how successful MDD treatment maps onto thalamic subnuclear connectivity and associated network-level function.

Supplementary data to this article can be found online at https://doi.org/10.1016/j.jad.2024.11.009.

Ethical statement

The medical ethical review board of the Amsterdam UMC (location VUmc) approved this study.

Funding

This research was funded by Amsterdam Neuroscience (Alliance Project Grant to M. Aghajani and G.A. van Wingen) and the Department of Psychiatry, Amsterdam UMC, Location VUmc.

CRediT authorship contribution statement

Weijian Liu: Writing - review & editing, Writing - original draft, Visualization, Software, Project administration, Methodology, Investigation, Formal analysis, Data curation, Conceptualization. Jurien Heij: Writing - review & editing, Methodology, Investigation. Shu Liu: Writing - review & editing, Methodology, Investigation. Luka Liebrand: Writing - review & editing, Project administration, Funding acquisition, Conceptualization. Matthan Caan: Writing - review & editing, Resources, Project administration, Funding acquisition. Wietske van der Zwaag: Writing – review & editing, Resources, Project administration, Funding acquisition. Dick J. Veltman: Writing – review & editing, Resources, Project administration, Funding acquisition. Lin Lu: Writing – review & editing, Validation, Supervision. Moji Aghajani: Writing - review & editing, Validation, Supervision, Resources, Project administration, Methodology, Funding acquisition, Data curation, Conceptualization. Guido van Wingen: Writing – review & editing, Validation, Supervision, Resources, Project administration, Methodol-Investigation, Funding acquisition, ogy, Conceptualization.

Declaration of competing interest

Matthan Caan is a shareholder of Nico-lab International Ltd. Guido van Wingen has received research support from Philips for unrelated work. The other authors declare that they have no conflict of interest.

Acknowledgements

The authors are extremely grateful to all participants involved in the study and gratefully acknowledge the contributions of SPINOZA Center for Neuroimaging Amsterdam and GGZ InGeest Amsterdam. Weijian Liu thanks Jorie (ZJC) for the recommendation of relevant literature.

Data availability

Data will be available from the corresponding author upon reasonable request.

References

Andersson, J.L.R., Sotiropoulos, S.N., 2016. An integrated approach to correction for offresonance effects and subject movement in diffusion MR imaging. NeuroImage 125, 1063–1078. https://doi.org/10.1016/j.neuroimage.2015.10.019.

Andersson, J.L.R., Skare, S., Ashburner, J., 2003. How to correct susceptibility distortions in spin-echo echo-planar images: application to diffusion tensor imaging. NeuroImage 20, 870–888. https://doi.org/10.1016/S1053-8119(03)00336-7.

Barson, J.R., Mack, N.R., Gao, W.-J., 2020. The paraventricular nucleus of the thalamus is an important node in the emotional processing network. Front. Behav. Neurosci. 14, 598469. https://doi.org/10.3389/fnbeh.2020.598469.

Basser, P.J., Mattiello, J., LeBihan, D., 1994a. Estimation of the effective self-diffusion tensor from the NMR spin echo. J. Magn. Reson. B 103, 247–254. https://doi.org/ 10.1006/jmrb.1994.1037.

Basser, P.J., Mattiello, J., LeBihan, D., 1994b. MR diffusion tensor spectroscopy and imaging. Biophys. J. 66, 259–267. https://doi.org/10.1016/S0006-3495(94)80775 1.

Beck, A.T., Epstein, N., Brown, G., Steer, R.A., 1988. An inventory for measuring clinical anxiety: psychometric properties. J. Consult. Clin. Psychol. 56, 893.
Belmaker, R.H., 2008. Major depressive disorder. N. Engl. J. Med. 14.

- Belujon, P., Grace, A.A., 2017. Dopamine system dysregulation in major depressive disorders. Int. J. Neuropsychopharmacol. 20, 1036–1046. https://doi.org/10.1093/ iing/pyx056
- Bhome, R., Zarkali, A., Thomas, G.E.C., Iglesias, J.E., Cole, J.H., Weil, R.S., 2022. Thalamic white matter macrostructure and subnuclei volumes in Parkinson's disease depression. NPJ Park. Dis. 8, 2. https://doi.org/10.1038/s41531-021-00270-y.
- Boelens Keun, J.T., van Heese, E.M., Laansma, M.A., Weeland, C.J., de Joode, N.T., van den Heuvel, O.A., Gool, J.K., Kasprzak, S., Bright, J.K., Vriend, C., van der Werf, Y. D., 2021. Structural assessment of thalamus morphology in brain disorders: a review and recommendation of thalamic nucleus segmentation and shape analysis. Neurosci. Biobehav. Rev. 131, 466–478. https://doi.org/10.1016/j.neubiorev.2021.09.044.
- Brown, E.C., Clark, D.L., Hassel, S., MacQueen, G., Ramasubbu, R., 2017.
 Thalamocortical connectivity in major depressive disorder. J. Affect. Disord. 217, 125–131. https://doi.org/10.1016/j.jad.2017.04.004.
- Caan, M.W.A., Bazin, P.-L., Marques, J.P., de Hollander, G., Dumoulin, S.O., van der Zwaag, W., 2019. MP2RAGEME: T1, T2*, and QSM mapping in one sequence at 7 tesla. Hum. Brain Mapp. 40, 1786–1798. https://doi.org/10.1002/hbm.24490.
- Casteen, E.J., Nielsen, S.R., Olson, E.A., Frederiks, K., Rosso, I.M., 2022. Reexperiencing and anxious arousal symptoms in relation to volumes of thalamus nuclei in posttraumatic stress spectrum adults. Brain Behav. 12, e2639. https://doi.org/ 10.1002/brb3.2639.
- Cattarinussi, G., Delvecchio, G., Maggioni, E., Bressi, C., Brambilla, P., 2021. Ultra-high field imaging in major depressive disorder: a review of structural and functional studies. J. Affect. Disord. 290, 65–73. https://doi.org/10.1016/j.jad.2021.04.056.
- Chen, G., 2022. Sources of information waste in neuroimaging: mishandling structures, thinking dichotomously, and over-reducing data. Aperture Neuro 2, 1–22. https://doi.org/10.52294/ApertureNeuro.2022.2.ZR.JI8542.
- Chen, G., Bürkner, P., Taylor, P.A., Li, Z., Yin, L., Glen, D.R., Kinnison, J., Cox, R.W., Pessoa, L., 2019a. An integrative Bayesian approach to matrix-based analysis in neuroimaging. Hum. Brain Mapp. 40, 4072–4090. https://doi.org/10.1002/ hbm.24686
- Chen, G., Xiao, Y., Taylor, P.A., Rajendra, J.K., Riggins, T., Geng, F., Redcay, E., Cox, R. W., 2019b. Handling multiplicity in neuroimaging through Bayesian lenses with multilevel modeling. Neuroinformatics 17. https://doi.org/10.1007/s12021-018-9409-6.
- Chen, G., Taylor, P.A., Cox, R.W., Pessoa, L., 2020. Fighting or embracing multiplicity in neuroimaging? Neighborhood leverage versus global calibration. NeuroImage 206, 116320. https://doi.org/10.1016/j.neuroimage.2019.116320.
- Cheng, W., Rolls, E.T., Qiu, J., Xie, X., Wei, D., Huang, C.-C., Yang, A.C., Tsai, S.-J., Li, Q., Meng, J., Lin, C.-P., Xie, P., Feng, J., 2018. Increased functional connectivity of the posterior cingulate cortex with the lateral orbitofrontal cortex in depression. Transl. Psychiatry 8, 1–10. https://doi.org/10.1038/s41398-018-0139-1.
- Chibaatar, E., Watanabe, K., Okamoto, N., Orkhonselenge, N., Natsuyama, T., Hayakawa, G., Ikenouchi, A., Kakeda, S., Yoshimura, R., 2023. Volumetric assessment of individual thalamic nuclei in patients with drug-naïve, first-episode major depressive disorder. Front. Psych. 14, 1151551. https://doi.org/10.3389/ fpsyt.2023.1151551.
- Coloigner, J., Batail, J.-M., Commowick, O., Corouge, I., Robert, G., Barillot, C., Drapier, D., 2019. White matter abnormalities in depression: a categorical and phenotypic diffusion MRI study. NeuroImage Clin. 22, 101710. https://doi.org/ 10.1016/j.nicl.2019.101710.
- Cordero-Grande, L., Christiaens, D., Hutter, J., Price, A.N., Hajnal, J.V., 2019. Complex diffusion-weighted image estimation via matrix recovery under general noise models. NeuroImage 200, 391–404. https://doi.org/10.1016/j. neuroImage.2019.06.039.
- Dailly, E., Chenu, F., Renard, C.E., Bourin, M., 2004. Dopamine, depression and antidepressants. Fundam. Clin. Pharmacol. 18, 601–607. https://doi.org/10.1111/ j.1472-8206.2004.00287.x.
- de Graaf, R., Bijl, R.V., Smit, F., Vollebergh, W.A.M., Spijker, J., 2002. Risk factors for 12-month comorbidity of mood, anxiety, and substance use disorders: findings from the Netherlands mental health survey and incidence study. Am. J. Psychiatry 159, 620–629. https://doi.org/10.1176/appi.ajp.159.4.620.
- De Marco, M., Manca, R., Mitolo, M., Venneri, A., 2017. White matter hyperintensity load modulates brain morphometry and brain connectivity in healthy adults: a neuroplastic mechanism? Neural Plast. 2017, 4050536. https://doi.org/10.1155/ 2017/4050536
- Dere, E., Pause, B.M., Pietrowsky, R., 2010. Emotion and episodic memory in neuropsychiatric disorders. Behav. Brain Res. 215, 162–171. https://doi.org/ 10.1016/j.bbr.2010.03.017. Special issue on episodic memory.
- Fischl, B., 2012. FreeSurfer. NeuroImage 62, 774–781. https://doi.org/10.1016/j.neuroimage.2012.01.021.
- Gallo, S., El-Gazzar, A., Zhutovsky, P., Thomas, R.M., Javaheripour, N., Li, M., Bartova, L., Bathula, D., Dannlowski, U., Davey, C., Frodl, T., Gotlib, I., Grimm, S., Grotegerd, D., Hahn, T., Hamilton, P.J., Harrison, B.J., Jansen, A., Kircher, T., Meyer, B., Nenadić, I., Olbrich, S., Paul, E., Pezawas, L., Sacchet, M.D., Sämann, P., Wagner, G., Walter, H., Walter, M., van Wingen, G., 2023. Functional connectivity signatures of major depressive disorder: machine learning analysis of two multicenter neuroimaging studies. Mol. Psychiatry 1–10. https://doi.org/10.1038/ pages 10.0021017.
- Godlewska, B.R., Browning, M., Norbury, R., Igoumenou, A., Cowen, P.J., Harmer, C.J., 2018. Predicting treatment response in depression: the role of anterior cingulate cortex. Int. J. Neuropsychopharmacol. 21, 988–996. https://doi.org/10.1093/ijnp/ pyy069.

- Grieve, S.M., Korgaonkar, M.S., Koslow, S.H., Gordon, E., Williams, L.M., 2013.
 Widespread reductions in gray matter volume in depression. NeuroImage Clin. 3, 332–339. https://doi.org/10.1016/j.nicl.2013.08.016.
- Hamilton, J.P., Etkin, A., Furman, D.J., Lemus, M.G., Johnson, R.F., Gotlib, I.H., 2012. Functional neuroimaging of major depressive disorder: a meta-analysis and new integration of base line activation and neural response data. Am. J. Psychiatry 169, 693–703. https://doi.org/10.1176/appi.ajp.2012.11071105.
- Hare, B.D., Duman, R.S., 2020. Prefrontal cortex circuits in depression and anxiety: contribution of discrete neuronal populations and target regions. Mol. Psychiatry 25, 2742–2758. https://doi.org/10.1038/s41380-020-0685-9.
- Hartikainen, K.M., Sun, L., Polvivaara, M., Brause, M., Lehtimäki, K., Haapasalo, J., Möttönen, T., Väyrynen, K., Ogawa, K.H., Öhman, J., Peltola, J., 2014. Immediate effects of deep brain stimulation of anterior thalamic nuclei on executive functions and emotion–attention interaction in humans. J. Clin. Exp. Neuropsychol. 36, 540–550. https://doi.org/10.1080/13803395.2014.913554.
- Heij, G.J., Penninx, B.W.H.J., van Velzen, L.S., van Tol, M.-J., van der Wee, N.J.A., Veltman, D.J., Aghajani, M., 2019. White matter architecture in major depression with anxious distress symptoms. Prog. Neuropsychopharmacol. Biol. Psychiatry 94, 109664. https://doi.org/10.1016/j.pnpbp.2019.109664.
- Heij, J., van der Zwaag, W., Knapen, T., Caan, M.W.A., Forstman, B., Veltman, D.J., van Wingen, G., Aghajani, M., 2024. Quantitative MRI at 7-Tesla reveals novel frontocortical myeloarchitecture anomalies in major depressive disorder. Transl. Psychiatry 14, 1–9. https://doi.org/10.1038/s41398-024-02976-y.
- Huang, L., Xi, Y., Peng, Y., Yang, Y., Huang, X., Fu, Y., Tao, Q., Xiao, J., Yuan, T., An, K., Zhao, H., Pu, M., Xu, F., Xue, T., Luo, M., So, K.-F., Ren, C., 2019. A visual circuit related to habenula underlies the antidepressive effects of light therapy. Neuron 102, 128–142.e8. https://doi.org/10.1016/j.neuron.2019.01.037.
- Iglesias, J.E., Insausti, R., Lerma-Usabiaga, G., Bocchetta, M., Van Leemput, K., Greve, D. N., van der Kouwe, A., Fischl, B., Caballero-Gaudes, C., Paz-Alonso, P.M., 2018. A probabilistic atlas of the human thalamic nuclei combining ex vivo MRI and histology. NeuroImage 183, 314–326. https://doi.org/10.1016/j.neuroimage.2018.08.012.
- Jenkinson, M., Smith, S., 2001. A global optimisation method for robust affine registration of brain images. Med. Image Anal. 5, 143–156. https://doi.org/ 10.1016/s1361-8415(01)00036-6.
- Jenkinson, M., Bannister, P., Brady, M., Smith, S., 2002. Improved optimization for the robust and accurate linear registration and motion correction of brain images. NeuroImage 17, 825–841. https://doi.org/10.1016/s1053-8119(02)91132-8.
- Jeurissen, B., Tournier, J.-D., Dhollander, T., Connelly, A., Sijbers, J., 2014. Multi-tissue constrained spherical deconvolution for improved analysis of multi-shell diffusion MRI data. NeuroImage 103, 411–426. https://doi.org/10.1016/j. neuroimage.2014.07.061.
- Kang, L., Zhang, A., Sun, N., Liu, P., Yang, C., Li, G., Liu, Z., Wang, Y., Zhang, K., 2018. Functional connectivity between the thalamus and the primary somatosensory cortex in major depressive disorder: a resting-state fMRI study. BMC Psychiatry 18, 339. https://doi.org/10.1186/s12888-018-1913-6.
- Keifer, O.P., Gutman, D.A., Hecht, E.E., Keilholz, S.D., Ressler, K.J., 2015. A comparative analysis of mouse and human medial geniculate nucleus connectivity: a DTI and anterograde tracing study. NeuroImage 105, 53–66. https://doi.org/10.1016/j. neuroImage 2014 10 047
- Kellner, E., Dhital, B., Kiselev, V.G., Reisert, M., 2016. Gibbs-ringing artifact removal based on local subvoxel-shifts. Magn. Reson. Med. 76, 1574–1581. https://doi.org/ 10.1002/mrm.26054
- Kempton, M.J., Salvador, Z., Munafo, M.R., Geddes, J.R., Simmons, A., Frangou, S., Williams, S.C., 2011. Structural neuroimaging studies in major depressive disorder. Meta-analysis and comparison with bipolar disorder. Arch. Gen. Psychiatry 68, 675–690. https://doi.org/10.1001/archgenpsychiatry.2011.60.
- Klein, M.O., Battagello, D.S., Cardoso, A.R., Hauser, D.N., Bittencourt, J.C., Correa, R.G., 2019. Dopamine: functions, signaling, and association with neurological diseases. Cell. Mol. Neurobiol. 39, 31–59. https://doi.org/10.1007/s10571-018-0632-3.
- Koolschijn, P.C.M.P., van Haren, N.E.M., Lensvelt-Mulders, G.J.L.M., Hulshoff Pol, H.E., Kahn, R.S., 2009. Brain volume abnormalities in major depressive disorder: a metaanalysis of magnetic resonance imaging studies. Hum. Brain Mapp. 30, 3719–3735. https://doi.org/10.1002/hbm.20801.
- Krauth, A., Blanc, R., Poveda, A., Jeanmonod, D., Morel, A., Székely, G., 2010. A mean three-dimensional atlas of the human thalamus: generation from multiple histological data. NeuroImage 49, 2053–2062. https://doi.org/10.1016/j. neuroImage.2009.10.042.
- Lai, C.H., Wu, Y.T., 2014. Alterations in white matter micro-integrity of the superior longitudinal fasciculus and anterior thalamic radiation of young adult patients with depression. Psychol. Med. 44, 2825–2832. https://doi.org/10.1017/ S0033291714000440.
- Lee, M.D., Wagenmakers, E.-J., 2014. Bayesian Cognitive Modeling: A Practical Course. Cambridge University Press.
- Levine, D.W., Kaplan, R.M., Kripke, D.F., Bowen, D.J., Naughton, M.J., Shumaker, S.A., 2003. Factor structure and measurement invariance of the Women's Health Initiative Insomnia Rating Scale. Psychol. Assess. 15, 123–136. https://doi.org/10.1037/ 1040-3590.15.2.123.
- Liebrand, L.C., van Wingen, G.A., Vos, F.M., Denys, D., Caan, M.W.A., 2020. Spatial versus angular resolution for tractography-assisted planning of deep brain stimulation. NeuroImage Clin. 25, 102116. https://doi.org/10.1016/j.nicl.2019.102116.
- Liu, T.T., Fu, J.Z., Chai, Y., Japee, S., Chen, G., Ungerleider, L.G., Merriam, E.P., 2022. Layer-specific, retinotopically-diffuse modulation in human visual cortex in response to viewing emotionally expressive faces. Nat. Commun. 13, 6302. https://doi.org/ 10.1038/s41467-022-33580-7.

- Liu, W., Heij, J., Liu, S., Liebrand, L., Caan, M., van der Zwaag, W., Veltman, D.J., Lu, L., Aghajani, M., van Wingen, G., 2024a. Hippocampal, thalamic, and amygdala subfield morphology in major depressive disorder: an ultra-high resolution MRI study at 7-Tesla. Eur. Arch. Psychiatry Clin. Neurosci. https://doi.org/10.1007/ s00406-024-01874-0.
- Liu, W., Heij, J., Liu, S., Liebrand, L., Caan, M., van der Zwaag, W., Veltman, D.J., Lu, L., Aghajani, M., van Wingen, G., 2024b. Structural connectivity of dopaminergic pathways in major depressive disorder: an ultra-high resolution 7-Tesla diffusion MRI study. Eur. Neuropsychopharmacol. 89, 58–70. https://doi.org/10.1016/j.europeuro.2024.07.014
- Malhi, G.S., Mann, J.J., 2018. Depression. Lancet 392, 2299–2312. https://doi.org/ 10.1016/s0140-6736(18)31948-2.
- Manjarrez, G., Herrera, R., Manjarrez, J., Mejenes, S., Hernandez-R, J., 2011. Functional change of the auditory cortex related to brain serotonergic neurotransmission in type 1 diabetic adolescents with and without depression. Eur. Psychiatry 26, 323. https:// doi.org/10.1016/S0924-9338(11)72032-6.
- Marques, J.P., Kober, T., Krueger, G., van der Zwaag, W., Van de Moortele, P.-F., Gruetter, R., 2010. MP2RAGE, a self bias-field corrected sequence for improved segmentation and T1-mapping at high field. NeuroImage 49, 1271–1281. https:// doi.org/10.1016/j.neuroimage.2009.10.002.
- Mayberg, H.S., Liotti, M., Brannan, S.K., McGinnis, S., Mahurin, R.K., Jerabek, P.A., Silva, J.A., Tekell, J.L., Martin, C.C., Lancaster, J.L., Fox, P.T., 1999. Reciprocal limbic-cortical function and negative mood: converging PET findings in depression and normal sadness. Am. J. Psychiatry 156, 675–682. https://doi.org/10.1176/ aip.156.5.675.
- Milaneschi, Y., Simmons, W.K., van Rossum, E.F.C., Penninx, B.W., 2019. Depression and obesity: evidence of shared biological mechanisms. Mol. Psychiatry 24, 18–33. https://doi.org/10.1038/s41380-018-0017-5.
- Mitchell, A.S., Gaffan, D., 2008. The magnocellular mediodorsal thalamus is necessary for memory acquisition, but not retrieval. J. Neurosci. 28, 258–263.
- Modha, D.S., Singh, R., 2010. Network architecture of the long-distance pathways in the macaque brain. Proc. Natl. Acad. Sci. U. S. A. 107, 13485–13490. https://doi.org/ 10.1073/pnas.1008054107.
- Morris, L.S., Kundu, P., Costi, S., Collins, A., Schneider, M., Verma, G., Balchandani, P., Murrough, J.W., 2019. Ultra-high field MRI reveals mood-related circuit disturbances in depression: a comparison between 3-tesla and 7-Tesla. Transl. Psychiatry 9, 94. https://doi.org/10.1038/s41398-019-0425-6.
- Murrough, J.W., Abdallah, C.G., Anticevic, A., Collins, K.A., Geha, P., Averill, L.A., Schwartz, J., DeWilde, K.E., Averill, C., Jia-Wei Yang, G., Wong, E., Tang, C.Y., Krystal, J.H., Iosifescu, D.V., Charney, D.S., 2016. Reduced global functional connectivity of the medial prefrontal cortex in major depressive disorder. Hum. Brain Mapp. 37, 3214–3223. https://doi.org/10.1002/hbm.23235.
- Novick, J.S., Cook, I.A., Rosenbaum, J.F., Balasubramani, G.K., Rush, A.J., 2005. Clinical and demographic features of atypical depression in outpatients with major depressive disorder: preliminary findings from STAR*D. J. Clin. Psychiatry. 66, 1002–1011. https://doi.org/10.4088/jcp.v66n0807.
- Nugent, A.C., Davis, R.M., Zarate, C.A., Drevets, W.C., 2013. Reduced thalamic volumes in major depressive disorder. Psychiatry Res. 213, 179–185. https://doi.org/ 10.1016/j.pscychresns.2013.05.004.
- Oke, A.F., Carver, L.A., Gouvion, C.M., Adams, R.N., 1997. Three-dimensional mapping of norepinephrine and serotonin in human thalamus. Brain Res. 763, 69–78. https:// doi.org/10.1016/s0006-8993(97)00404-6.
- Otte, C., Gold, S.M., Penninx, B.W., Pariante, C.M., Etkin, A., Fava, M., Mohr, D.C., Schatzberg, A.F., 2016. Major depressive disorder. Nat Rev Primer 2, 16065. https://doi.org/10.1038/nrdp.2016.65.
- Ouhaz, Z., Fleming, H., Mitchell, A.S., 2018. Cognitive functions and neurodevelopmental disorders involving the prefrontal cortex and mediodorsal thalamus. Front. Neurosci. 12, 33
- Pan, P.M., Sato, J.R., Salum, G.A., Rohde, L.A., Gadelha, A., Zugman, A., Mari, J., Jackowski, A., Picon, F., Miguel, E.C., Pine, D.S., Leibenluft, E., Bressan, R.A., Stringaris, A., 2017. Ventral striatum functional connectivity as a predictor of adolescent depressive disorder in a longitudinal community-based sample. Am. J. Psychiatry 174, 1112–1119. https://doi.org/10.1176/appi.ajp.2017.17040430.
- Pan, P.M., Sato, J.R., Paillère Martinot, M.-L., Martinot, J.-L., Artiges, E., Penttilä, J., Grimmer, Y., van Noort, B.M., Becker, A., Banaschewski, T., Bokde, A.L.W., Desrivières, S., Flor, H., Garavan, H., Ittermann, B., Nees, F., Papadopoulos Orfanos, D., Poustka, L., Fröhner, J.H., Whelan, R., Schumann, G., Westwater, M.L., Grillon, C., Cogo-Moreira, H., Stringaris, A., Ernst, M., 2022. Longitudinal trajectory of the link between ventral striatum and depression in adolescence. Am. J. Psychiatry 179, 470–481. https://doi.org/10.1176/appi.ajp.20081180.
- Pessoa, L., 2017. A network model of the emotional brain. Trends Cogn. Sci. 21, 357–371. https://doi.org/10.1016/j.tics.2017.03.002.
- Pittenger, C., Duman, R.S., 2008. Stress, depression, and neuroplasticity: a convergence of mechanisms. Neuropsychopharmacology 33, 88–109. https://doi.org/10.1038/sj. npp.1301574.
- Pizzagalli, D.A., Roberts, A.C., 2022. Prefrontal cortex and depression. Neuropsychopharmacology 47, 225–246. https://doi.org/10.1038/s41386-021-01101-7.
- Polders, D.L., Leemans, A., Hendrikse, J., Donahue, M.J., Luijten, P.R., Hoogduin, J.M., 2011. Signal to noise ratio and uncertainty in diffusion tensor imaging at 1.5, 3.0, and 7.0 Tesla. J. Magn. Reson. Imaging 33, 1456–1463. https://doi.org/10.1002/ jmrl.22554.
- Rush, A.J., Gullion, C.M., Basco, M.R., Jarrett, R.B., Trivedi, M.H., 1996. The Inventory of Depressive Symptomatology (IDS): psychometric properties. Psychol. Med. 26, 477–486. https://doi.org/10.1017/s0033291700035558.

- Saalmann, Y.B., Pinsk, M.A., Wang, L., Li, X., Kastner, S., 2012. The pulvinar regulates information transmission between cortical areas based on attention demands. Science 337, 753–756. https://doi.org/10.1126/science.1223082.
- Schmidt, F.M., Sander, C., Dietz, M.-E., Nowak, C., Schröder, T., Mergl, R., Schönknecht, P., Himmerich, H., Hegerl, U., 2017. Brain arousal regulation as response predictor for antidepressant therapy in major depression. Sci. Rep. 7, 45187. https://doi.org/10.1038/srep45187.
- Shen, X., Adams, M.J., Ritakari, T.E., Cox, S.R., McIntosh, A.M., Whalley, H.C., 2019. White matter microstructure and its relation to longitudinal measures of depressive symptoms in mid- and late life. Biol. Psychiatry 86, 759–768. https://doi.org/10.1016/j.biopsych.2019.06.011.
- Smeets, R.M.W., Dingemans, P., 1993. Composite International Diagnostic Interview (CIDI), Version 1.1. World Health Organ. AmsterdamGeneva.
- Smith, S.M., Jenkinson, M., Woolrich, M.W., Beckmann, C.F., Behrens, T.E.J., Johansen-Berg, H., Bannister, P.R., De Luca, M., Drobnjak, I., Flitney, D.E., Niazy, R.K., Saunders, J., Vickers, J., Zhang, Y., De Stefano, N., Brady, J.M., Matthews, P.M., 2004. Advances in functional and structural MR image analysis and implementation as FSL. NeuroImage 23 (Suppl. 1), S208–S219. https://doi.org/10.1016/j.neuroImage.2004.07.051.
- Smith, R.E., Tournier, J.-D., Calamante, F., Connelly, A., 2012. Anatomically-constrained tractography: improved diffusion MRI streamlines tractography through effective use of anatomical information. NeuroImage 62, 1924–1938. https://doi.org/ 10.1016/j.neuroimage.2012.06.005.
- Smith, R.E., Tournier, J.-D., Calamante, F., Connelly, A., 2013. SIFT: spherical-deconvolution informed filtering of tractograms. NeuroImage 67, 298–312. https://doi.org/10.1016/j.neuroimage.2012.11.049.
- Smith, R.E., Tournier, J.-D., Calamante, F., Connelly, A., 2015. SIFT2: enabling dense quantitative assessment of brain white matter connectivity using streamlines tractography. NeuroImage 119, 338–351. https://doi.org/10.1016/j. neuroimage.2015.06.092.
- Spellman, T., Liston, C., 2020. Toward circuit mechanisms of pathophysiology in depression. Am. J. Psychiatry 177, 381–390. https://doi.org/10.1176/appi. aip.2020.20030280.
- Steriade, M., Glenn, L.L., 1982. Neocortical and caudate projections of intralaminar thalamic neurons and their synaptic excitation from midbrain reticular core. J. Neurophysiol. 48, 352–371. https://doi.org/10.1152/jn.1982.48.2.352.
- Strotmann, B., Heidemann, R.M., Anwander, A., Weiss, M., Trampel, R., Villringer, A., Turner, R., 2014. High-resolution MRI and diffusion-weighted imaging of the human habenula at 7 tesla. J. Magn. Reson. Imaging 39, 1018–1026. https://doi.org/10.1002/imri.24252.
- Sun, L., Peräkylä, J., Polvivaara, M., Öhman, J., Peltola, J., Lehtimäki, K., Huhtala, H., Hartikainen, K.M., 2015. Human anterior thalamic nuclei are involved in emotion–attention interaction. Neuropsychologia 78, 88–94. https://doi.org/ 10.1016/j.neuropsychologia.2015.10.001.
- Surova, G., Ulke, C., Schmidt, F.M., Hensch, T., Sander, C., Hegerl, U., 2021. Fatigue and brain arousal in patients with major depressive disorder. Eur. Arch. Psychiatry Clin. Neurosci. 271, 527–536. https://doi.org/10.1007/s00406-020-01216-w.
- Neurosci. 271, 527–536. https://doi.org/10.1007/s00406-020-01216-w.
 Tadayonnejad, R., Ajilore, O., Mickey, B.J., Crane, N.A., Hsu, D.T., Kumar, A.,
 Zubieta, J.-K., Langenecker, S.A., 2016. Pharmacological modulation of pulvinar
 resting-state regional oscillations and network dynamics in major depression.
 Psychiatry Res. 252, 10–18. https://doi.org/10.1016/j.pscychresns.2016.04.013.
- Takano, A., Varrone, A., Gulyás, B., Karlsson, P., Tauscher, J., Halldin, C., 2008. Mapping of the norepinephrine transporter in the human brain using PET with (S, S)-[18F] FMeNER-D2. Neuroimage 42, 474–482.
- Tamura, T., Sugihara, G., Okita, K., Mukai, Y., Matsuda, H., Shiwaku, H., Takagi, S., Daisaki, H., Tateishi, U., Takahashi, H., 2022. Dopamine dysfunction in depression: application of texture analysis to dopamine transporter single-photon emission computed tomography imaging. Transl. Psychiatry 12, 1–7. https://doi.org/10.1038/s41398-022-02080-z.
- Tan, J., Ye, L., 2023. The thalamic-primary auditory cortex circuit: a pathway to resilience in the face of stress and a potential target for depression treatment. Chin. J. Nat. Med. 21, 801–803. https://doi.org/10.1016/S1875-5364(23)60447-9.
- Tournier, J.-D., Calamante, F., Connelly, A., 2010. Improved probabilistic streamlines tractography by 2nd order integration over fibre orientation distributions. In: Proc Intl Soc Mag Reson Med ISMRM 18.
- Tournier, J.-D., Smith, R., Raffelt, D., Tabbara, R., Dhollander, T., Pietsch, M., Christiaens, D., Jeurissen, B., Yeh, C.-H., Connelly, A., 2019. MRtrix3: a fast, flexible and open software framework for medical image processing and visualisation. NeuroImage 202, 116137. https://doi.org/10.1016/j.neuroimage.2019.116137.
- Tustison, N.J., Avants, B.B., Cook, P.A., Zheng, Y., Egan, A., Yushkevich, P.A., Gee, J.C., 2010. N4ITK: improved N3 bias correction. IEEE Trans. Med. Imaging 29, 1310–1320. https://doi.org/10.1109/TMI.2010.2046908.
- van de Schoot, R., Kaplan, D., Denissen, J., Asendorpf, J.B., Neyer, F.J., van Aken, M.A. G., 2014. A gentle introduction to Bayesian analysis: applications to developmental research. Child Dev. 85, 842–860. https://doi.org/10.1111/cdev.12169.
- van Doorn, J., van den Bergh, D., Böhm, U., Dablander, F., Derks, K., Draws, T., Etz, A., Evans, N.J., Gronau, Q.F., Haaf, J.M., Hinne, M., Kucharský, Š., Ly, A., Marsman, M., Matzke, D., Gupta, A.R.K.N., Sarafoglou, A., Stefan, A., Voelkel, J.G., Wagenmakers, E.-J., 2021. The JASP guidelines for conducting and reporting a Bayesian analysis. Psychon. Bull. Rev. 28, 813–826. https://doi.org/10.3758/s13423-020-01798-5.
- van Velzen, L.S., Kelly, S., Isaev, D., Aleman, A., Aftanas, L.I., Bauer, J., Baune, B.T., Brak, I.V., Carballedo, A., Connolly, C.G., Couvy-Duchesne, B., Cullen, K.R., Danilenko, K.V., Dannlowski, U., Enneking, V., Filimonova, E., Förster, K., Frodl, T., Gotlib, I.H., Groenewold, N.A., Grotegerd, D., Harris, M.A., Hatton, S.N., Hawkins, E. L., Hickie, I.B., Ho, T.C., Jansen, A., Kircher, T., Klimes-Dougan, B., Kochunov, P.,

- Krug, A., Lagopoulos, J., Lee, R., Lett, T.A., Li, M., MacMaster, F.P., Martin, N.G., McIntosh, A.M., McLellan, Q., Meinert, S., Nenadić, I., Osipov, E., Penninx, B.W.J.H., Portella, M.J., Repple, J., Roos, A., Sacchet, M.D., Sämann, P.G., Schnell, K., Shen, X., Sim, K., Stein, D.J., van Tol, M.-J., Tomyshev, A.S., Tozzi, L., Veer, I.M., Vermeiren, R., Vives-Gilabert, Y., Walter, H., Walter, M., van der Wee, N.J.A., van der Werff, S.J.A., Schreiner, M.W., Whalley, H.C., Wright, M.J., Yang, T.T., Zhu, A., Veltman, D.J., Thompson, P.M., Jahanshad, N., Schmaal, L., 2020. White matter disturbances in major depressive disorder: a coordinated analysis across 20 international cohorts in the ENIGMA MDD working group. Mol. Psychiatry 25, 1511–1525. https://doi.org/10.1038/s41380-019-0477-2.
- Veraart, J., Sijbers, J., Sunaert, S., Leemans, A., Jeurissen, B., 2013. Weighted linear least squares estimation of diffusion MRI parameters: strengths, limitations, and pitfalls. NeuroImage 81, 335–346. https://doi.org/10.1016/j.neuroimage.2013.05.028.
- Veraart, J., Fieremans, E., Novikov, D.S., 2016a. Diffusion MRI noise mapping using random matrix theory. Magn. Reson. Med. 76, 1582–1593. https://doi.org/10.1002/ mrm 26059
- Veraart, J., Novikov, D.S., Christiaens, D., Ades-Aron, B., Sijbers, J., Fieremans, E., 2016b. Denoising of diffusion MRI using random matrix theory. NeuroImage 142, 394–406. https://doi.org/10.1016/j.neuroimage.2016.08.016.
- Vertes, R.P., Linley, S.B., Rojas, A.K.P., 2022. Structural and functional organization of the midline and intralaminar nuclei of the thalamus. Front. Behav. Neurosci. 16, 964644. https://doi.org/10.3389/fnbeh.2022.964644.
- Vu, A.T., Auerbach, E., Lenglet, C., Moeller, S., Sotiropoulos, S.N., Jbabdi, S., Andersson, J., Yacoub, E., Ugurbil, K., 2015. High resolution whole brain diffusion imaging at 7 T for the Human Connectome Project. Neuroimage 122, 318–331.
- Wang, Y.-B., Song, N.-N., Ding, Y.-Q., Zhang, L., 2023. Neural plasticity and depression treatment. IBRO Neurosci. Rep. 14, 160–184. https://doi.org/10.1016/j. ibneur 2022 09 001

- World Health Organization, 2008. The Global Burden of Disease: 2004 Update. World Health Organization.
- Xiong, G., Dong, D., Cheng, C., Jiang, Y., Sun, X., He, J., Li, C., Gao, Y., Zhong, X., Zhao, H., Wang, X., Yao, S., 2021. Potential structural trait markers of depression in the form of alterations in the structures of subcortical nuclei and structural covariance network properties. NeuroImage Clin. 32, 102871. https://doi.org/10.1016/i.nicl.2021.102871.
- Yang, C., Xiao, K., Ao, Y., Cui, Q., Jing, X., Wang, Y., 2022. The thalamus is the causal hub of intervention in patients with major depressive disorder: evidence from the granger causality analysis. NeuroImage Clin. 37, 103295. https://doi.org/10.1016/j. nicl.2022.103295.
- Young, K.A., Holcomb, L.A., Yazdani, U., Hicks, P.B., German, D.C., 2004. Elevated neuron number in the limbic thalamus in major depression. Am. J. Psychiatry 161, 1270–1277. https://doi.org/10.1176/appi.ajp.161.7.1270.
- Young, K.A., Holcomb, L.A., Bonkale, W.L., Hicks, P.B., Yazdani, U., German, D.C., 2007. 5HTTLPR polymorphism and enlargement of the pulvinar: unlocking the backdoor to the limbic system. Biol. Psychiatry 61, 813–818.
- Zhang, F., Peng, W., Sweeney, J.A., Jia, Z., Gong, Q., 2018. Brain structure alterations in depression: psychoradiological evidence. CNS Neurosci. Ther. 24, 994–1003. https://doi.org/10.1111/cns.12835.
- Zhang, Yuxuan, Zhang, Yingli, Ai, H., Van Dam, N.T., Qian, L., Hou, G., Xu, P., 2022. Microstructural deficits of the thalamus in major depressive disorder. Brain Commun. 4, fcac236. https://doi.org/10.1093/braincomms/fcac236.
- Zheng, W., Tan, X., Liu, T., Li, X., Gao, J., Hong, L., Zhang, X., Zhao, Z., Yu, Y., Zhang, Y., Luo, B., Wu, D., 2021. Individualized thalamic parcellastion reveals alterations in shape and microstructure of thalamic nuclei in patients with disorder of consciousness. Cereb. Cortex Commun. 2, tgab024. https://doi.org/10.1093/texcom/tgab024.